PHILOSOPHICAL TRANSACTIONS OF THE ROYAL SOCIETY A MATHEMATICAL, PHYSICAL & ENGINEERING SCIENCES

The Effect of Shear on Thermotropic Liquid Crystalline Polymers

L. Gervat, M. R. Mackley, T. M. Nicholson and A. H. Windle

Phil. Trans. R. Soc. Lond. A 1995 **350**, 1-27
doi: 10.1098/rsta.1995.0001

The effect of shear on thermotropic liquid crystalline polymers

By L. Gervat†, M. R. Mackley, T. M. Nicholson‡ and A. H. Windle

Departments of Chemical Engineering and of Materials Science and Metallurgy, University of Cambridge, Pembroke Street, Cambridge CB2 3RA, U.K.

We present and review optical and rheological data on a number of sheared thermotropic liquid crystal polymers LCPs. Optical observations were carried out by using a shearing apparatus that was designed for these and additional *in situ* X-ray measurements. X-ray data on sheared LCPs are also presented together with orientation relaxation measurements made on the cessation of flow.

To reconcile the optical, X-ray and rheological data, a numerical scheme is constructed that can qualitatively, and in some cases quantitatively predict observed behaviour. Essential elements of the model are concerned with a local molecular anisotropy, a molecular correlation coefficient, and a local defect structure. The model shows, among other predictions, that stress relaxation is essentially decoupled from both orientation and optical relaxation. In addition the presence of a defect texture influences orientation aspects more than the rheology.

1. Introduction

Molten thermotropic liquid crystalline polymers have physical properties which have been separately related to the modelling of small molecule liquid crystals and flexible chain polymers. In this paper we attempt to reconcile both viewpoints and initially we briefly review relevant aspects relating to both individual classes of material.

In relation to small molecule liquid crystals (SMLCs), the underlying basis for their modelling is to consider the material's local anisotropy, which can be described in terms of an order parameter (see, for example, de Gennes 1974; Chandrasekhar 1977). The local orientation of the ordering is usually described by a director, and it was established at an early stage that topological irregularities, or defects, often exist within this anisotropic material (Lehman 1890). These defects have been mathematically predicted (Frank 1958) and have become known as disclinations. The rheology of defect free SMLCs can be successfully described by a continuum theory which uses anisotropic viscosity and elasticity coefficients (Leslie 1983) although a continuum model of flow that includes the presence of disclinations has not yet been successfully achieved. The origin of elasticity

† Present address: Elf Atochem, 90 Rue Danton, 42300 Levallois, Perret, France.
‡ Present address: IRC in Polymer Science and Technology, University of Leeds, Leeds LS2 9JT, U.K.

Phil. Trans. R. Soc. Lond. A (1995) **350**, 1–27
Printed in Great Britain

within a SMLC comes from the splay twist and bend distortions proposed by Frank (1958).

In relation to molten flexible polymers, it is now generally accepted that they exist as interpenetrating random coils (see, for example, Flory 1969). When subject to shear, the chains are perturbed from their random configuration and the resultant orientation and rheology of the material is a reflection of the competition between elastic entropic deformation and viscous relaxation. Doi & Edwards (1986) have successfully constructed a molecular theory based on the concept of reptation, and this theory can explain many of their rheological features. The importance of a spectrum of relaxation times within the linear viscoelastic response of a polydisperse material has been appreciated by many (Ferry 1961; Baumgaertel & Winter 1989; Kamath & Mackley 1989) and the nonlinear rheological response of the material can be realistically described in terms of a damping function, which was a concept introduced by Wagner (1979) and extended by others (see, for example, Wissbrun & Dealy 1990).

In 1976 Eastman Kodak reported the discovery of a thermotropic liquid crystal polyester known as X7G (Jackson & Kuhfus 1976) and since then a broad range of experimental studies have been carried out on, in particular, the Hoechst-Celanese Vectra LCP, as this material is one of a very limited number of commercially available variants.

With certain important exceptions, the rheology of thermotropic liquid crystalline polymers (TLCPs) appears to be similar to that of molten flexible polymers. They show a similar linear viscoelastic response and their shear thinning characteristics, to a first approximation, can be modelled in a similar way to molten polymers (Guskey & Winter 1991). They do, however, show differences, such as a near complete absence of die swell when extruded through a capillary (Done & Baird 1987) and in addition the material does not show high flow rate global melt instabilities such as the shark skin effect or discontinuities in the capillary flow curve.

On the other hand, optical textures of TLCPs have been observed by a number of workers (see, for example, Mackley *et al.* 1981; Viney *et al.* 1983*b*; Graziano & Mackley 1984*a*; Alderman & Mackley 1985; Sawyer & Jaffe 1986) and these optical textures correspond more closely to SMLCs than to flexible polymers. The two underlying features observed in molten TLCPs is that of optical birefringence coupled with strong light scattering. Birefringence is present in the quiescent state and relates directly to the intrinsic local anisotropy of the material (Mackley *et al.* 1981). The light scattering is associated with sudden changes in the refractive index gradient within the material and under certain conditions this has been correlated by Graziano & Mackley (1984*a*) and Alderman & Mackley (1985) with a line disclination structure. Some of these line defects have been subsequently modelled by Nicholson (1989) and the similarity to SMLC defect behaviour shown by Graziano & Mackley (1984*b*).

In a number of cases the optical scattering texture of TLCPs in the molten state is dominant and the length scale of the scattering entities is close to the resolution of the optical microscope. This texture has been called a tight texture (Viney *et al.* 1983*b*), a dense defect texture (Alderman & Mackley 1985), or a polydomain (Chapoy *et al.* 1988).

In contrast, molten flexible polymers in the quiescent state are generally optically transparent and structure free. They develop birefringence when sheared,

which subsequently relaxes with a certain timescale on the cessation of shear (Tanaka *et al.* 1989). There is a direct correlation with optical and stress response through the stress optical coefficient of the material, and generally the material response to flow deformation is well understood.

When TLCPs are sheared, dramatic changes in optical textures can be seen and these features will be summarized in later sections of this paper. In addition, under certain conditions, on the cessation of shear a banded texture has been observed (Viney *et al.* 1983*a*; Graziano & Mackley 1984*a*), while subsequent heat treatment can reveal a rich spectrum of textures (Viney *et al.* 1985).

X-ray studies offer a potentially useful way of examining anisotropy within samples, however, up to this point most observations on TLCPs have been limited to the quiescent state (see, for example, Blundell *et al.* 1982), or to examining the orientation developed in samples cooled after being drawn or sheared at elevated temperatures (Mitchell & Windle 1982; Done & Baird 1987). In relation to flowing LCPs, work has only been performed on lyotropic polymers, where the shear may be imposed at room temperature (Doppert & Picken 1987; Keates *et al.* 1992).

Concerning the mathematical modelling of liquid crystal polymers, most previous attempts have concentrated on lyotropic systems. Doi has developed a defect free model for rodlike entities (see, for example, Doi & Edwards 1986) and Larson & Mead (1989) have proposed a polydomain phenomenological description of lyotropic systems. Marrucci & Maffettone (1990) solved a diffusion equation for rodlike lyotropic molecules and the model predicts a low shear tumbling régime for the director trajectory and a higher shear alignment régime. Recently Doi has presented the mathematical framework for modelling the rheology of mesoscopic domain structures (Doi 1992) and Larson *et al.* (1992) have extended their experimental observations and scaling arguments on lyotropic systems.

The purpose of this paper is to review our own experimental observations on optical, X-ray and rheological measurements of TLCPs and link these observations with those of other workers to give an overview of the response of the material to shear. We then construct a numerical scheme that is capable of describing most of the gross features associated with the observed behaviour. The problem is itself complex because local anisotropy, rheology and defect textures all play an interconnected role, and in order to make the problem tractable, each element has had to be introduced in a simple way. In § 2 experimental procedures are described and in §§ 3, 4 and 5 the experimental optical, X-ray and rheological data respectively are given. In § 6 the numerical scheme together with its predictions is presented and finally in § 7 the successes and limitations of the model are discussed.

2. Materials and experimental procedure

(*a*) *Materials used*

Most experiments were carried out on a random copolyester composed of 73% hydroxybenzoic acid and 27% hydroxynaphthoic acid supplied by Hoechst-Celanese and designated Polymer A (see figure 1*a*). This material forms a mobile liquid crystal melt at temperatures above about 295 °C. It is sensitive to temperature and cannot exist above 320 °C for any extended period without chemical modification. The molecular mass averages are unknown, although the zero shear viscosity reported later is substantial and of order 10^5 Pa s suggesting that the polymer has a significant degree of polymerization with $\overline{\mathrm{DP}_n}$ certainly above 100.

PHILOSOPHICAL TRANSACTIONS OF THE ROYAL SOCIETY A MATHEMATICAL, PHYSICAL & ENGINEERING SCIENCES

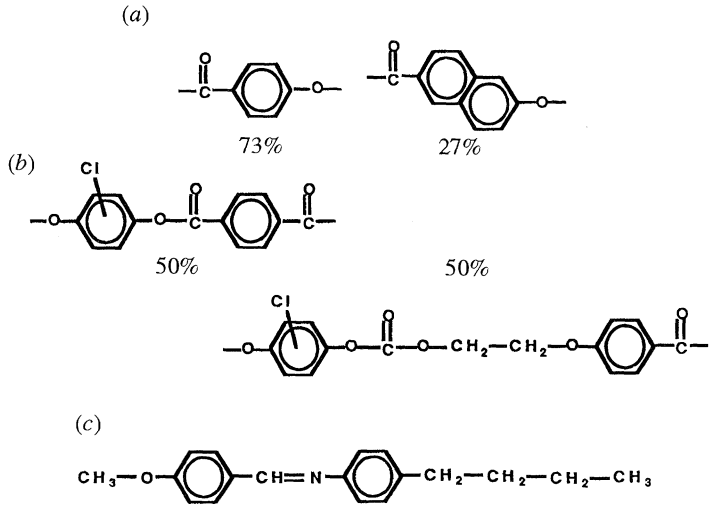

Figure 1. Chemical structures of materials used. (*a*) Polymer A and (*b*) Polymer B are thermotropic liquid crystal polymers. (*c*) MBBA is a small molecule liquid crystal.

Some optical observations are reported for an ICI development grade copolyester designated Polymer B. The chemical composition of this chlorinated material is shown in figure 1*b* and the material forms a mobile mesophase above about 200 °C. Finally in terms of TLCPs an optical texture of a Rhone Poulenc development grade copolyester is also included. It is a random copolyester formed from dicarboxy diphenylether, terephthalic acid, paracetoxybenzoic acid and methylhydroquinone and is designated Polymer C.

As a basis for comparison with SMLC behaviour, a series of photographs for 4-methoxybenzylidene-4-*n*-butyl aniline (MBBA) is also given. The chemical structure of MBBA is shown in figure 1*c* and the material is a nematic at room temperature.

(*b*) *Optical shearing apparatus*

Optical observations were made in two custom built shear cells, one of which has previously been described (Alderman & Mackley 1985). This device imposes a translational oscillatory linear shear deformation on a sample placed between two heated glass discs. A maximum amplitude of 1 mm and frequencies of 0.02–6 s^{-1} are possible.

In the course of the current series of experiments we have developed a new rotational shear cell which is shown schematically in figure 2 and in the photograph of figure 3. The sample, a hot-pressed polymer disc of 29 mm diameter by about 50 μm thick, is held between two circular glass discs, one of which is rotated with respect to the other. Observations are made through a 5 mm diameter port positioned towards the circumference of the discs where the deformation of the sample may be considered closely linear. A microcomputer controlled stepper motor system allows steady rotation speeds between 0.02 and 10 rad s^{-1}. Oscillatory motion with amplitudes of between 0.005 and 5 rad at frequencies of between 0.5 and 5 cycles s^{-1} is also possible.

The polymer sample is heated by foil heaters behind the glass windows. These can reach operational temperatures of up to 350 °C rapidly and maintain a uniform temperature over the working area of the window (±2 °C at a nominal

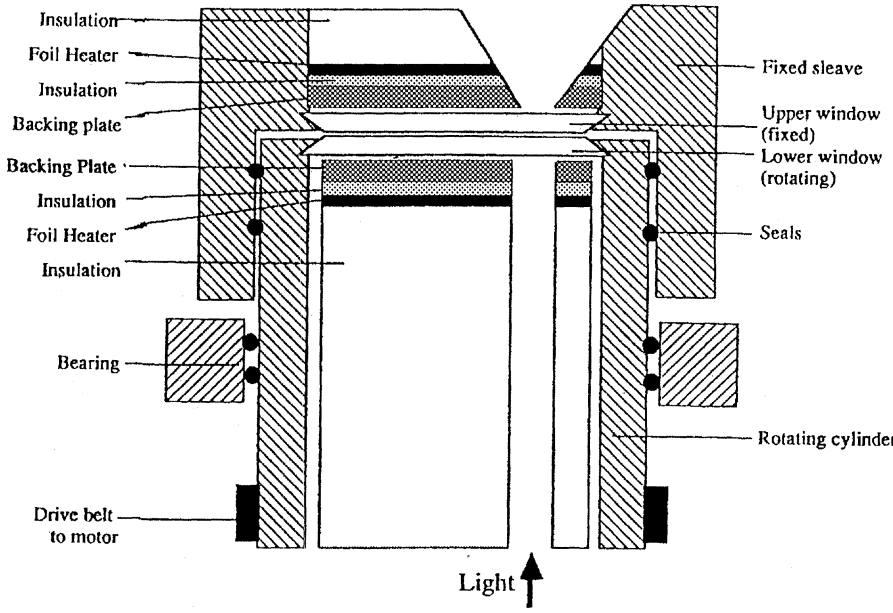

Figure 2. Cross-sectional diagram of rotational shear cell.

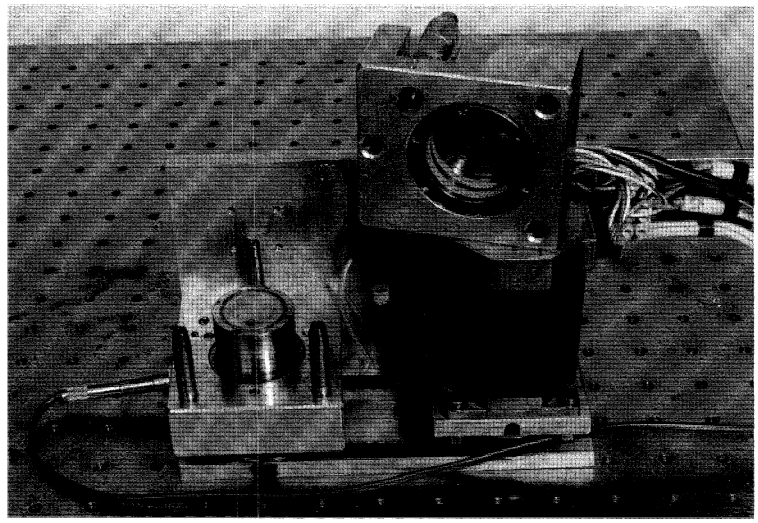

Figure 3. Photograph of the rotational shear cell with the upper, stationary, window assembly removed.

temperature of 300 °C). The design of the cell ensures that the two windows remain parallel, the distance between them being measured by a micrometer.

As with the translational shear cell, observations were made with a modified Swift microscope between crossed polarizers using a ×20 long working distance objective.

(*c*) *X-ray measurements*

Replacing the glass discs with mica or polyimide film windows, the new rotational shear cell may be used to observe X-ray diffraction patterns from molten

PHILOSOPHICAL TRANSACTIONS OF THE ROYAL SOCIETY A MATHEMATICAL, PHYSICAL & ENGINEERING SCIENCES

LCP samples while they are being sheared. In order to obtain a stronger diffraction pattern the sample thickness was increased to 1 mm.

Initial observations were made using a conventional CuK_α source, the patterns being collected on flat film, taking about 30 min for an exposure. It was possible to observe reflections at Bragg angles of up to $2\theta = 25°$. To allow time resolved observations of the change in the diffraction pattern after the cessation of shear, a high intensity synchrotron source at the SERC Daresbury Laboratory was used. Here area detectors allowed a diffraction pattern to be recorded in under 1 min.

(*d*) *Rheological measurements*

The characterization of the rheology of the liquid crystalline polymer was performed on a Rheometrics, Dynamic Spectrometer II, using parallel plate and cone and plate geometry. Samples were hot-pressed discs of Polymer A, 25 mm diameter by 1 mm thick, and experiments were performed at 310 °C.

Three different deformation types were used.

(i) *Small strain oscillatory deformation*

A small oscillatory shear strain ($\gamma = \gamma_0 \sin \omega t$) is applied to the lower plate. From the torque $T(t)$ measured on the upper plate the stress response $\tau(t)$ is calculated and divided into two components: in and out of phase with the applied strain. Two moduli may therefore be defined:

$$\tau(t) = \gamma_0 (G' \sin \omega t + G'' \cos \omega t), \tag{2.1}$$

where G' is the storage (elastic) modulus and G'' the loss (viscous) modulus.

(ii) *Step strain*

A finite shear strain γ_0 is rapidly applied to the lower plate. The stress generated is measured and related to the relaxation modulus:

$$G(t) = \tau(t)/\gamma_0, \tag{2.2}$$

where $\tau(t)$ is the time response of the stress after the step strain deformation. This may be performed for a range of strains, but at lower strains (less than 5%) the results suffer from noise as the measured torques can be very low.

(iii) *Steady shear*

A constant shear rate is applied to the bottom plate and the resulting stress measured. Of interest is both the steady stress level as a function of applied strain rate, and the form of the growth of the stress to a steady value and its subsequent relaxation upon cessation of shear. The results have a tendency to be noisy because of the large scale deformations being applied to the sample.

3. Optical observations

Small molecule liquid crystals such as MBBA are excellent candidates for optical observation because the structures within the fluid can usually be readily identified and the effect of shear observed without ambiguity. In figure 4 we show the evolution of a MBBA sample when subjected to shear in the rotational optical shearing apparatus. Figure 4*a* shows the material in the initial quiescent state and within the bulk of the sample a few disclination loops can be seen. When

PHILOSOPHICAL TRANSACTIONS OF THE ROYAL SOCIETY A MATHEMATICAL, PHYSICAL & ENGINEERING SCIENCES

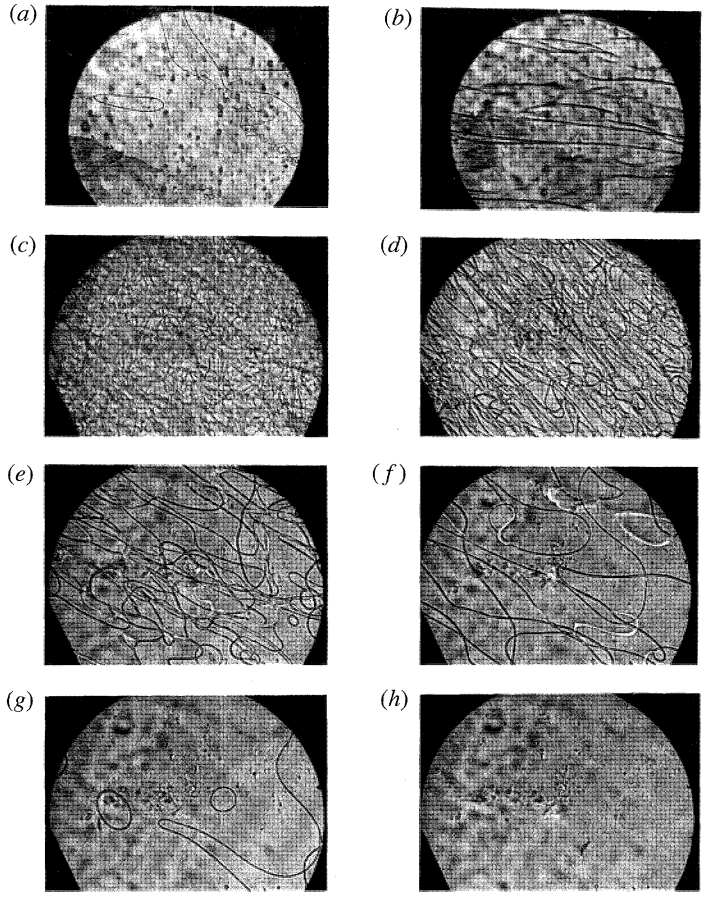

Figure 4. Micrographs of MBBA. (*a*) At rest. (*b*) Shear rate $10\,s^{-1}$. (*c*) Shear rate $100\,s^{-1}$. (*d*) 5s, (*e*) 10 s, (*f*) 30 s, (*g*) 1 min and (*h*) 2 min after cessation of shear. Direction of shear is horizontal.

the material is subjected to a steady shear of $\sim 10\,s^{-1}$ these disclination loops distort within the shear (figure 4*b*). However, at a higher shear rate ($\sim 100\,s^{-1}$) disclination multiplication occurs and the disclinations align in the direction of flow as shown in figure 4*c*. On cessation of flow (figure 4*d*) the 'dense array' of disclinations relax to a more isotropic configuration and with subsequent elapse of time shown in figure 4*e*–*h* the line defects relax, in this case to a final defect free state shown in figure 4*h*. The dominant feature is generation of disclination loops during shear and their subsequent relaxation on the cessation of shear. The observations reported here are consistent and compliment those reported earlier by Graziano & Mackley (1984*b*). They are also supported by the optical observations of Hilltrop & Fischer (1976) who observed preferred orientation at low shear rates and disclination multiplication at high shear.

The optical textures observed in TLCPs are often more complex and difficult to interpret. Figure 5 shows the typical quiescent optical texture for three TLCPs. Figure 5*a* corresponds to Polymer B, figure 5*b* to Polymer C and figure 5*c* to Polymer A. Each polymer shows significant scattering either when viewed between crossed polaroids or in bright field and the general texture appears to be

PHILOSOPHICAL TRANSACTIONS OF THE ROYAL SOCIETY A MATHEMATICAL, PHYSICAL & ENGINEERING SCIENCES

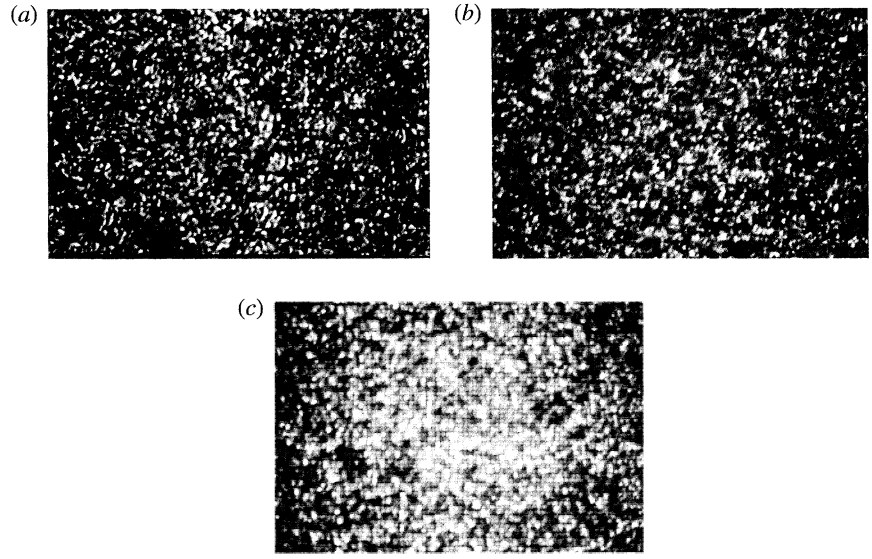

Figure 5. Dense defect textures. All viewed between crossed polars. Thickness *ca.* 40 μm, width of photo 250 μm. Annealing time 1 min. (*a*) Polymer B 220 °C, (*b*) Polymer C 315 °C, (*c*) Polymer A 310 °C.

insensitive to the differences of the chemical repeat unit in each case. The probable origin of these textures can be seen by annealing the sample at elevated temperature but without shear. Figure 6 shows the annealing process for Polymer B at a temperature of 220 °C. With time the original texture coarsens and by the photograph of figure 6*d*, which was taken after 12 min, the texture has relaxed sufficiently to reveal the presence of line defects. In figure 6*e* disclination loops are clearly visible and after 20 min (figure 6*f*) the defect structure has completely disappeared. From observations such as these it would appear that the photographs shown in figure 5 and figure 6*a* are directly linked with a dense defect structure. Again these observations are consistent with those reported by Alderman & Mackley (1985). In the case of Polymer A, which lacks the flexible spacers between the meseogenic units present in Polymer B, relaxation of the dense texture is still observed, but on a longer timescale.

The shearing behaviour of TLCPs can depend on the initial state of the material. Starting with a dense defect texture shown in figure 7*a*, shearing causes this texture to be modified by the distortion and multiplication of the defect texture, as indicated in figure 7*b*. Further shearing at higher rates leads to the apparent disappearance of any defect textures and the emergence of pure birefringence with the optic axis in the plane of shear (figure 7*c*). On the cessation of shear, the material will relax back to the original dense defect state with a relaxation time that depends both on the polymer and the temperature. Typically this might range from a few seconds to tens of minutes. In some situations the material may relax through a banded texture (Graziano & Mackley 1984*a*).

We now follow the effect of shear on Polymer B when its starting state is defect free due to prior annealing. The defect free state is shown in figure 8*a*. With the imposition of shear, shown in figure 8*b*, *c*, defects are generated during the shearing process. Most, if not all, of the defects appear to be disclination loops. At higher shear rates, shown in figure 8*d*, the defect texture again appears

PHILOSOPHICAL TRANSACTIONS OF THE ROYAL SOCIETY A MATHEMATICAL, PHYSICAL & ENGINEERING SCIENCES

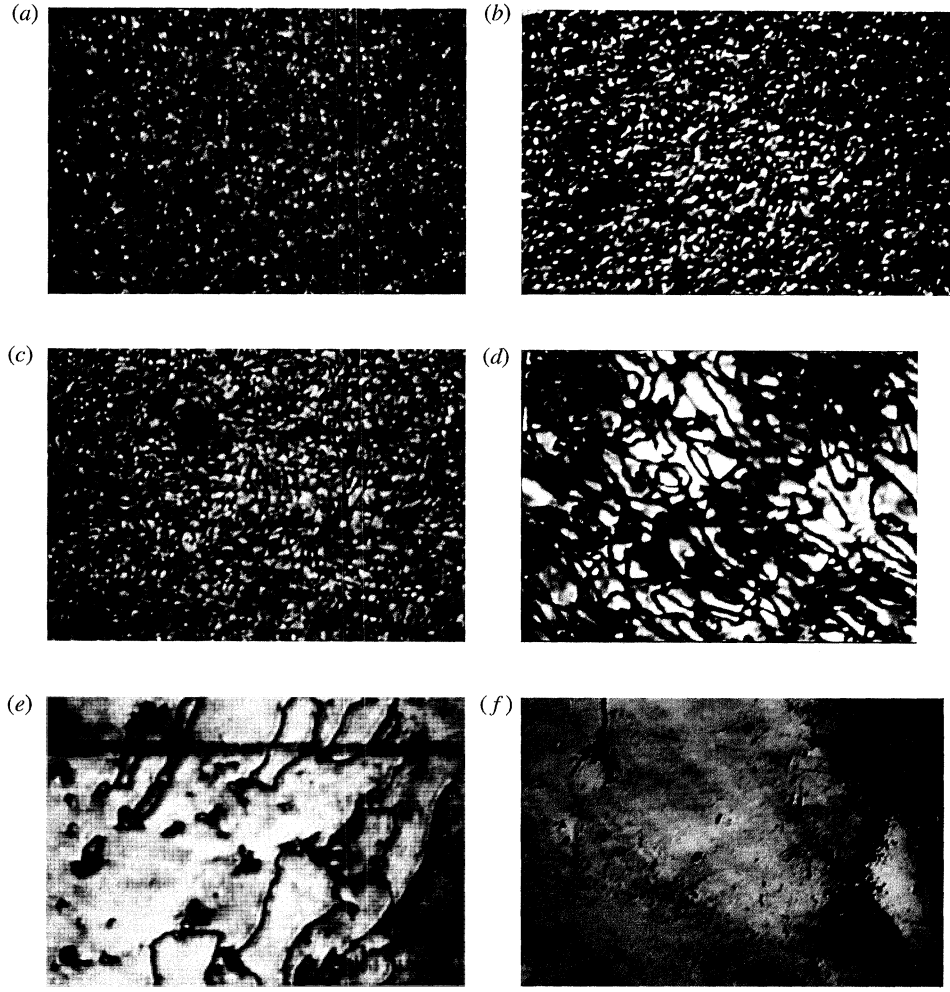

Figure 6. Annealing of dense defect textures in Polymer B. All viewed between crossed polars. Thickness *ca.* 40 μm, width of photo 250 μm. T = 220 °C. (*a*) 1 min, (*b*) 5 min, (*c*) 10 min, (*d*) 12 min, (*e*) 15 min, (*f*) 20 min.

to be lost leaving pure birefringence contrast only. On the cessation of shear the oriented defect texture reappears and is observed to relax and coarsen with time.

In summary for TLCPs we observe quite generally an initial dense defect state that can in principle be removed with thermal annealing. Shearing of the dense defect state leads to defect modification and at high shear rates the optical disappearance of the dense structure leaving evidence of orientation alone. On cessation of flow, the material usually returns to the dense defect state. If the material starts defect free, shear induces defect creation and subsequent orientation. On the cessation of shear the material returns to its defect free state.

4. X-ray observations

A limited number of *in situ* X-ray diffraction measurements of the degree of preferred orientation in Polymer A were carried out at 310 °C using the rotational

PHILOSOPHICAL TRANSACTIONS OF THE ROYAL SOCIETY A MATHEMATICAL, PHYSICAL & ENGINEERING SCIENCES

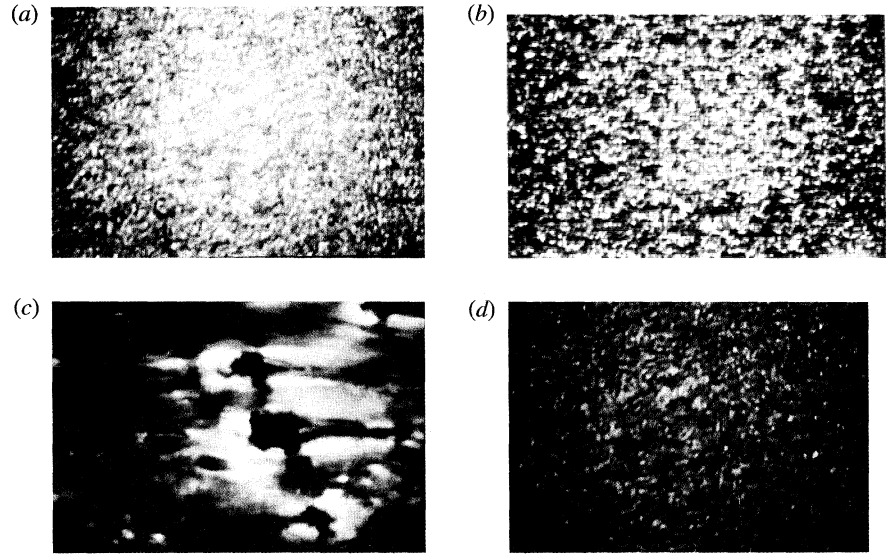

Figure 7. The effect of shear on dense defect state in Polymer B 220 °C All viewed between crossed polars at 45° to horizontal oscillatory shear. Thickness *ca.* 40 μm, width of photo 250 μm, annealing time 1 min. (*a*) Quiescent state, (*b*) maximum shear rate 5 s^{-1}, (*c*) maximum shear rate 150 s^{-1}, (*d*) 1 s after shear at 150 s^{-1}.

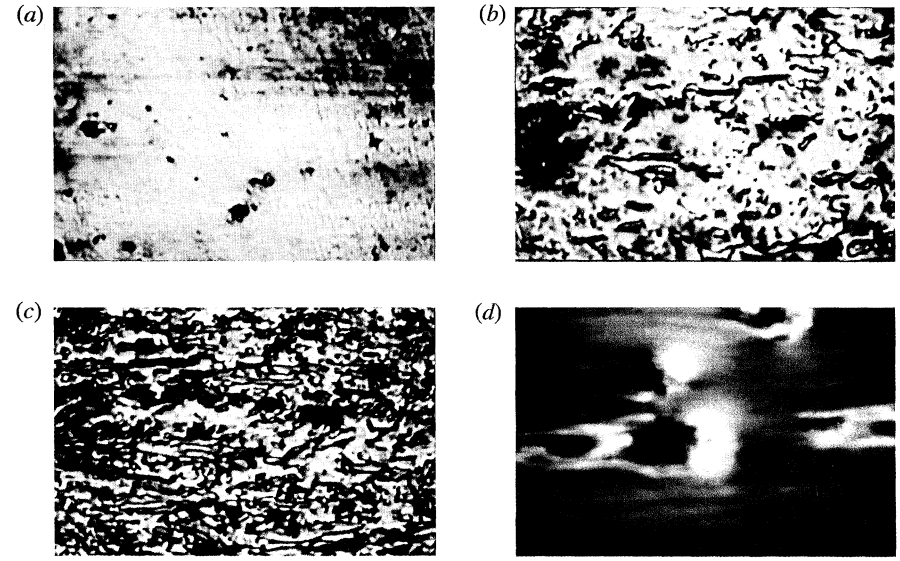

Figure 8. The effect of shear on defect free state in Polymer B at 220 °C. All viewed between crossed polars at 45° to horizontal oscillatory shear. Thickness *ca.* 40 μm, width of photo 250 μm, annealing time 20 min. (*a*) Quiescent stage, (*b*) maximum shear rate 1 s^{-1}, (*c*) maximum shear rate 10 s^{-1}, (*d*) maximum shear rate 150 s^{-1}.

shearing apparatus and the Daresbury synchrotron X-ray source. Photographs of the observed diffraction patterns are shown in figure 9. Figure 9*a* corresponds to a state before shear. The pattern is dominated by the essentially uniform intensity diffraction arc at $2\theta = 18.6°$. With the application of steady shear (figure 9*b*, *c*, which is horizontal in the figure, evidence for orientation is seen

PHILOSOPHICAL TRANSACTIONS OF THE ROYAL SOCIETY A MATHEMATICAL, PHYSICAL & ENGINEERING SCIENCES

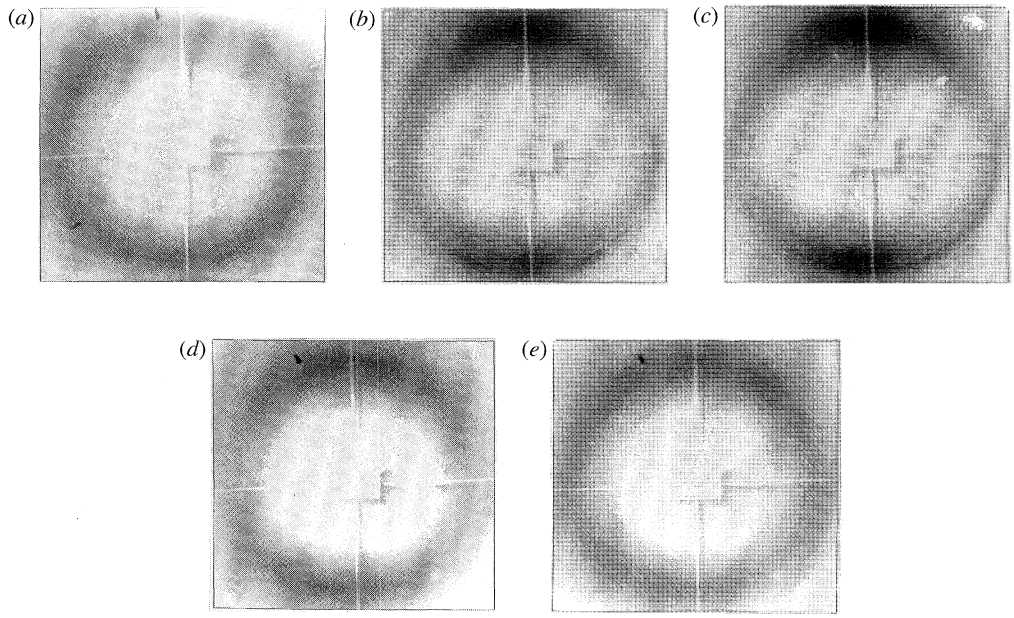

Figure 9. Diffraction patterns of Polymer A collected at the Daresbury SRS. The shear direction is horizontal. Temperature 310 °C. (*a*) At rest. (*b*) Shear rate $2\,s^{-1}$. (*c*) Shear rate $20\,s^{-1}$. (*d*) 2 min and (*e*) 9 min after cessation of shear.

with a concentration of the diffraction peak intensity on the equator. With the cessation of flow (figure 9*d*, *e*) the orientation is observed to relax over a period, which for the conditions reported here, was of about 9 min.

The main feature of all these patterns is the diffuse diffraction ring at an angle of $2\theta = 18.6°$. This corresponds to the approximate interchain periodicity in the polymer and for a fully aligned sample would give rise to two more or less equal regions of intensity positioned symmetrically on the equator. The more intense meridional reflection observed in these polymers (Mitchell & Windle 1982) is at a higher 2θ angle and cannot be observed with the shear cell in its current configuration.

The degree of orientation in the sample is quantified by measuring the intensity of the X-ray scattering around this ring of constant diffraction angle as a function of azimuthal angle ϕ. This is corrected for the effects of background scattering from an empty shear cell and for the absorption of X-rays by the polymer. An orientation function is calculated:

$$S = \int_0^{2\pi} I(\phi) P_2(\phi)\,\mathrm{d}\phi \Big/ \int_0^{2\pi} I(\phi)\,\mathrm{d}\phi, \tag{4.1}$$

where $I(\phi)$ is the intensity at an azimuthal angle of ϕ and P_2 is the second Legendre polynomial, $P_2(\phi) = \frac{1}{2}(3\cos^2\phi - 1)$ (see, for example, Windle 1982; Mitchell & Windle 1988).

Results of the analysis of the diffraction patterns of figure 9 are given in table 1. The synchrotron X-ray data reveal orientation information alone without the complication of direct observation of the defect texture. The orientation in the unsheared sample may be accounted for by the inevitable shear deformations

Table 1. *Orientation functions calculated from the diffraction patterns of figure 9*

ref		$S_{\text{amorphous}}$	S_{crystal}
(*a*)	no shear	0.30	
(*b*)	shear $2\,s^{-1}$	0.70	0.65
(*c*)	shear $20\,s^{-1}$	0.80	0.68
(*d*)	relax 2 min	0.48	
(*e*)	relax 9 min	0.34	

imposed by hot-pressing during the preparation of the sample. It is clearly seen that shear induces some orientation in the sample but, even at the higher rate, orientation is far from complete. If it were, an orientation function of $S = 1$ would be obtained. The maximum value of $S = 0.8$ reported here is quite modest. By comparison, tensile drawing followed by quenching can give orientations of the crystalline component which closely approaches unity (Mitchell & Windle 1988) whereas the same polymer of a somewhat lower molecular mass has been oriented in a magnetic field of 5.6 T to $S = 0.97$ (Anwer & Windle 1993). Relaxation of orientation after cessation of shear takes place over a relatively long timescale of the order of several minutes.

There is also some evidence from the diffraction patterns taken during shear in figure 9*b*, *c* for the formation of crystallites. This is seen as the development of a sharp (in the radial direction) diffraction arc at a higher diffraction angle (19.4°) than the amorphous liquid crystalline diffraction. Figure 10*a* shows intensity scans along the equator for the diffraction patterns of figure 9 showing the development of the additional crystal peak. This is seen more clearly in an intensity scan along the meridian of the diffraction patterns (figure 10*b*) since the crystal diffraction does not orient as much as the liquid crystalline diffraction. Upon cessation of shear the crystalline diffraction disappears rapidly. It is thought that this is due to the formation and rapid remelting of non-periodic layer crystals (Nicholson *et al.* 1992). Orientation functions for crystalline components, where observed, are included in table 1.

The X-ray data compliments the optical observations and gives direct orientation information. In addition the X-ray relaxation of orientation after cessation of shear seems to occur over a similar timescale to the optical relaxation of textures observed for this material at the same temperature.

5. Rheology

In this section we present the rheology of Polymer A at one temperature of 310 °C. This material has been studied by a number of workers (Lin & Winter 1988; Troughton *et al.* 1989; Cocchine *et al.* 1991) and in general our results are consistent with theirs. The rheology of the material is very sensitive to temperature, particularly below the temperature chosen here.

(*a*) *Oscillatory measurements*

Small strain oscillatory data were obtained over a frequency range of $\omega = 0.01$–$500\,\text{rad}\,s^{-1}$. The data points in figure 11 show the classical response of a

PHILOSOPHICAL TRANSACTIONS OF THE ROYAL SOCIETY A MATHEMATICAL, PHYSICAL & ENGINEERING SCIENCES

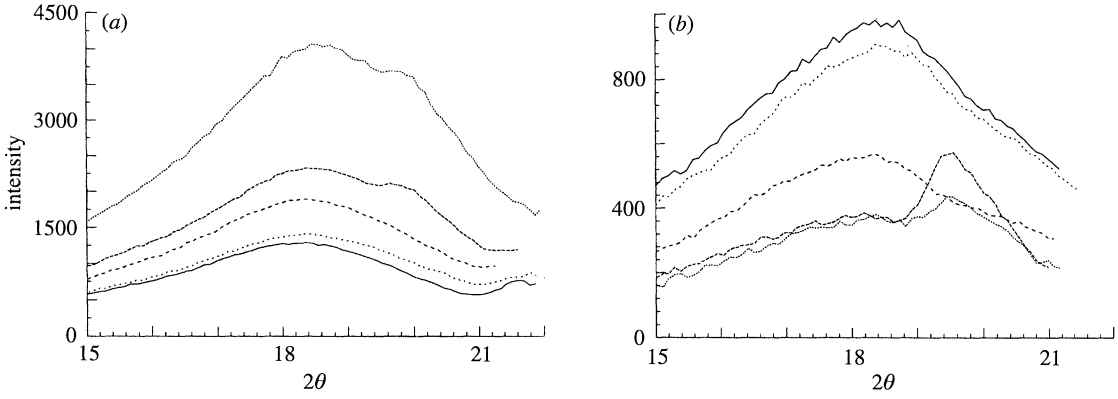

Figure 10. Radial scans (2θ) through the diffraction patterns of figure 9. (a) Vertical scan (along the equator). (b) Horizontal scans (along the meridian). ———, figure 9a; - - - - -, figure 9b; · · · · · ·, figure 9c; - - -, figure 9d; · · ·, figure 9e.

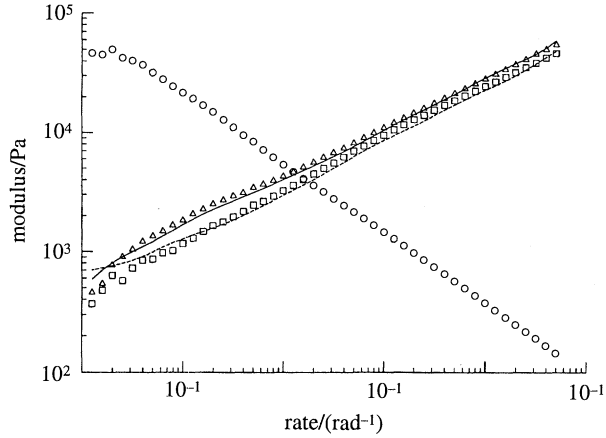

Figure 11. Small strain dynamic rheology of Polymer A. Temperature 310 °C,strain 1%. △, Storage modulus, G'; □, loss modulus, G''; ○, complex viscosity; η^*. The lines were calculated from Maxwell model equations (5.1) and (5.2) using the best fit values of the moduli shown in figure 12; ———, G'; - - - - -, G''.

conventional flexible polymer melt in that G' and G'' are of the same order of magnitude and they both increase with increasing frequency. There is also some evidence to suggest that a plateau behaviour is seen for the complex viscosity η^* where $\eta^* = \sqrt{(G'^2 + G''^2)}/\omega$.

These data can be fitted to a Maxwell type model which describes linear viscoelastic materials in terms of a time constant λ and a modulus G. For an LCP a single time constant is not sufficient to describe the data and so a series of Maxwell elements with varying time constants are used. The dynamic storage and loss moduli are related to the time constants and moduli by the expressions,

$$G'(\omega) = \sum_i \frac{G_i \omega^2 \lambda_i^2}{1 + \omega^2 \lambda_i^2}, \tag{5.1}$$

$$G''(\omega) = \sum_i \frac{G_i \omega \lambda_i}{1 + \omega^2 \lambda_i^2}. \tag{5.2}$$

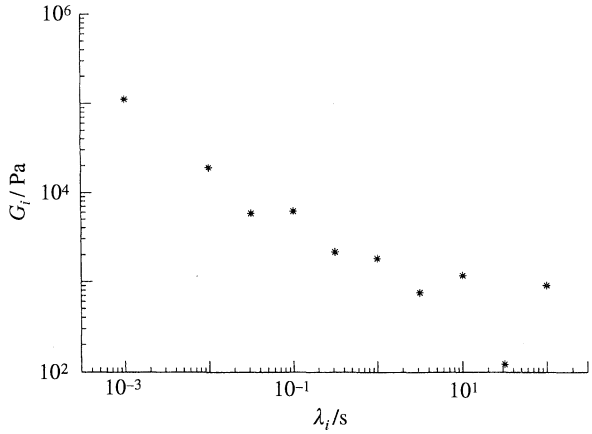

Figure 12. Moduli of Maxwell elements used to fit the data of figure 11.

Eleven time constants, logarithmically spread over the range 10^{-3} to 10^2 are chosen and the corresponding moduli calculated by a least squares method. The resulting moduli are shown in figure 12 as a function of the time constant. The lines in figure 11 were calculated from these moduli using the formulae of equations (5.1) and (5.2) to provide an indication of the success of the Maxwell model fit to the experimental data.

The fitting of Maxwell elements to the G', G'' data has been discussed in a number of papers (Baumgaertel & Winter 1989; Kamath & Mackley 1989). No method is without error, however, the choice of 11 time constants over a broad range of timescales gives a good fit to the data as shown in figure 11.

(*b*) *Step strain*

Step strain data for Polymer A is shown in figure 13 for a range of strains. For small strains the relaxation modulus is linear on a log–log plot with a relatively long time constant for the relaxation. At higher strains two regions are evident; a dramatic strain softening at short times followed by a longer relaxation of comparable time constant to that observed at small strains.

For a system of Maxwell elements representing a viscoelastic material, the relaxation of the system following a step strain deformation may be derived from the constitutive equation as

$$G_0(t) = \frac{\tau(t)}{\gamma} = \sum_i G_i \mathrm{e}^{-t/\lambda_i}, \tag{5.3}$$

where G_i and λ_i are the moduli and time constants for the Maxwell elements and γ the magnitude of the step strain. Figure 13 includes a line corresponding to the $G_0(t)$ generated from the G' and G'' data and agreement between the two sets of data is considered acceptable. The fall off in the Maxwell element predicted modulus at long times is due to the lack of very low frequency data in the dynamic experiments.

This, however, shows no dependence of relaxation modulus upon strain, so a damping function is added to the constitutive equation leading to a new expres-

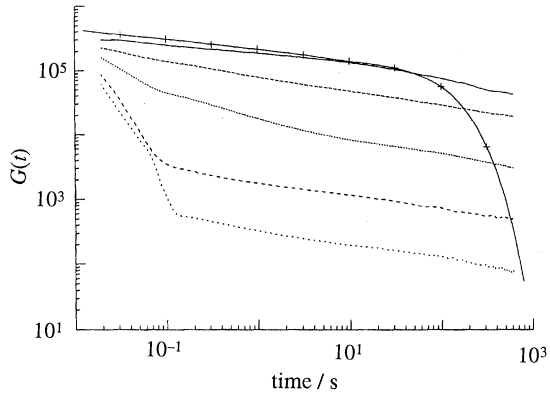

Figure 13. Relaxation moduli for Polymer A calculated from step strain experiments at 310 °C. Temperature 310 °C. ———, 3% Strain; - - - - -, 10% strain; · · · · · ·, 30% strain; - - -, 100% strain; · · ·, 300% strain. Superimposed is the relaxation modulus calculated, using equation (5.3), from the Maxwell elements moduli, —+—+—,.

sion for the relaxation modulus

$$G_\gamma(t) = \mathrm{e}^{-k\gamma} \sum_i G_i \mathrm{e}^{-t/\lambda_i}. \tag{5.4}$$

This has proved successful for conventional melts (see, for example, Wagner 1979; Kamath & Mackley 1990), indicating in these instances that the constitutive equation is factorable into strain and time dependencies, and that a single value for the damping coefficient k can be found.

However, for the Polymer A data, the degree of damping is clearly dependent on both time and strain so such an approach will be less successful. Using the longer time relaxation data from figure 13 damping coefficients in the range $k = 2$–4.6 are obtained.

These values of k, together with those of G_i and λ_i obtained from the dynamic measurements may be used to calculate relaxation moduli, assuming the form of response given in equation (5.4). This is compared with the original data in figure 14. Over the central time region good agreement is found, but deviations occur at both short and long times. The long time deviation is again due to the absence of very low frequency data in the dynamic experiments. At short times, and high strains the response is clearly not factorable.

(*c*) *Steady shear*

Figure 15 shows the variation in the magnitude of the steady shear stress response as a function of strain rate. On a log–log plot this is approximately linear and shows a power law behaviour, $\tau = k\dot{\gamma}^n$, with a power law index of 0.6. This is a similar response to that observed in a conventional polymer melt.

The time dependence of the steady shear response is shown in figure 16. A common feature is the stress overshoot that occurs before the steady shear stress level is attained. Stress relaxation occurs over a time of about 5 s. From these data alone it is clear that the timescales for stress relaxation and orientation relaxation, as measured using X-rays, are very different.

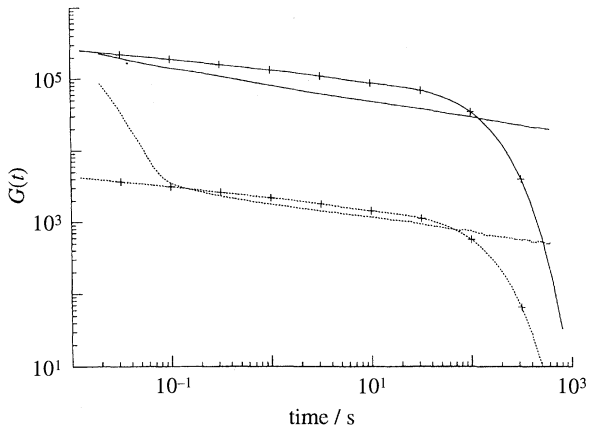

Figure 14. Experimental relaxation moduli from figure 13: ———, 10% strain; ·····, 100% strain; together with calculated step strain data using equation (5.4): —+—+—, 10% strain; ·+···+·, 100% strain. Damping coefficient k fixed at 4.6.

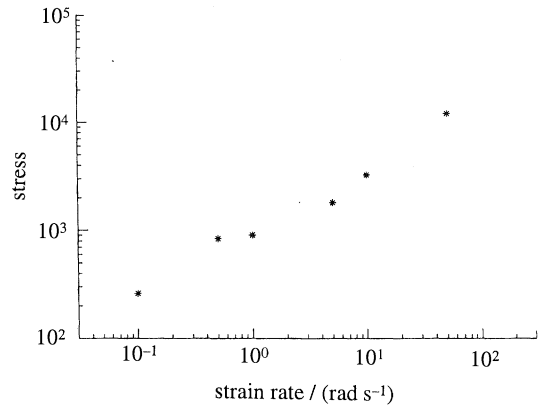

Figure 15. Steady shear stress values for Polymer A as a function of shear rate.

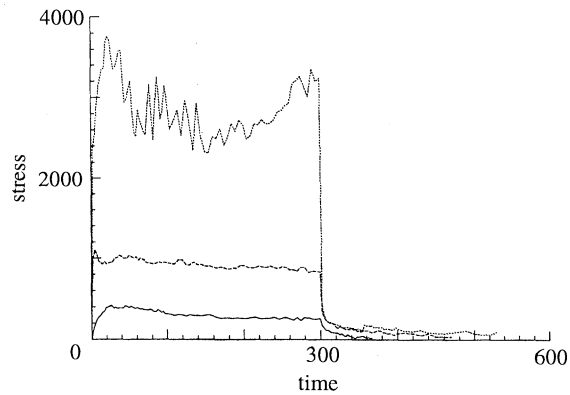

Figure 16. Stress growth against relaxation curves for Polymer A. Shear ceased at 300 s. Temperature 310 °C. ———, 0.1 s^{-1}; - - - - -, 1 s^{-1}; ·····, 10 s^{-1}.

PHILOSOPHICAL TRANSACTIONS OF THE ROYAL SOCIETY A MATHEMATICAL, PHYSICAL & ENGINEERING SCIENCES

6. Simulation of microstructure and rheology

A supramolecular lattice simulation has been developed in an attempt to model the optical microstructures in liquid crystal systems (Nicholson 1989; Bedford *et al.* 1991). Here this simulation is developed to model the effect of shear on the liquid crystal structures and their resulting rheological properties. We wish for example to predict both stress and orientational relaxation behaviour from the same model and have a scheme that is also self-consistent with the optical observations.

(*a*) *Definition of lattice and equilibrium configuration*

Initially the material is divided up into a periodic array of cells placed on a two- or three-dimensional lattice. Each cell is characterized by a single direction which is assumed to be related to the molecular director (the preferred local orientation of chain axes). This is assumed to be uniform in a single cell (that is the *local* orientation is $S = 1$), but may vary from cell to cell (so the *global* orientation may be less than unity). Initially the directors are assigned random directions. Simulations reported in this paper were performed on a 50×50 array and periodic boundary conditions were used with no external constraints present.

As described by Bedford *et al.* (1991) the lowest energy state for two adjacent cells is when their orientations are parallel. The orientation of a single cell which minimizes its energy can be shown to be the average of the orientation of its immediate neighbours. At each stage in the simulation therefore the orientation of each cell is moved a fraction of its deviation from this mean neighbourhood orientation:

$$\boldsymbol{x}_{n+1} = (1 - \rho)\boldsymbol{x}_n + \rho\overline{\boldsymbol{x}}, \tag{6.1}$$

where the vectors $\boldsymbol{x}_n$ and $\boldsymbol{x}_{n+1}$ represent successive orientations of a cell, $\overline{\boldsymbol{x}}$ the average neighbourhood cell orientation and ρ a correlation coefficient, which in this paper was fixed at 0.2.

Figure 17 shows the effect of applying this director correlation process alone to an initially random array of directors. In figure 17*a* the initial random set of directors can be seen. The situation shown in figure 17*b* corresponds to one iteration step using equation (6.1). Figures 17*c*–*f* correspond to 2, 5, 10 and 50 subsequent iterations. From these pictures it can be seen that after about ten iterations the director map reaches a steady state and the map shows local regions of correlated orientation together with a local defect texture. The model to a first approximation therefore simulates, at stages during its development, local anisotropy and defects, as observed experimentally. The exact nature of the final director maps will depend on the initial conditions of the director and the value of the chosen correlation coefficient.

(*b*) *The effect of shear*

Shear is modelled by applying incremental pseudo-affine deformations. The directions of the vectors representing the directors in the cells are deformed as if they were embedded in a solid undergoing an affine deformation with the desired shear increment, but any length changes in these vectors are ignored. Cell positions are also changed by the deformation, subject to the cells always remaining on lattice sites. In setting up the model in this way, the possibility of director tumbling is ruled out.

PHILOSOPHICAL TRANSACTIONS OF THE ROYAL SOCIETY A MATHEMATICAL, PHYSICAL & ENGINEERING SCIENCES

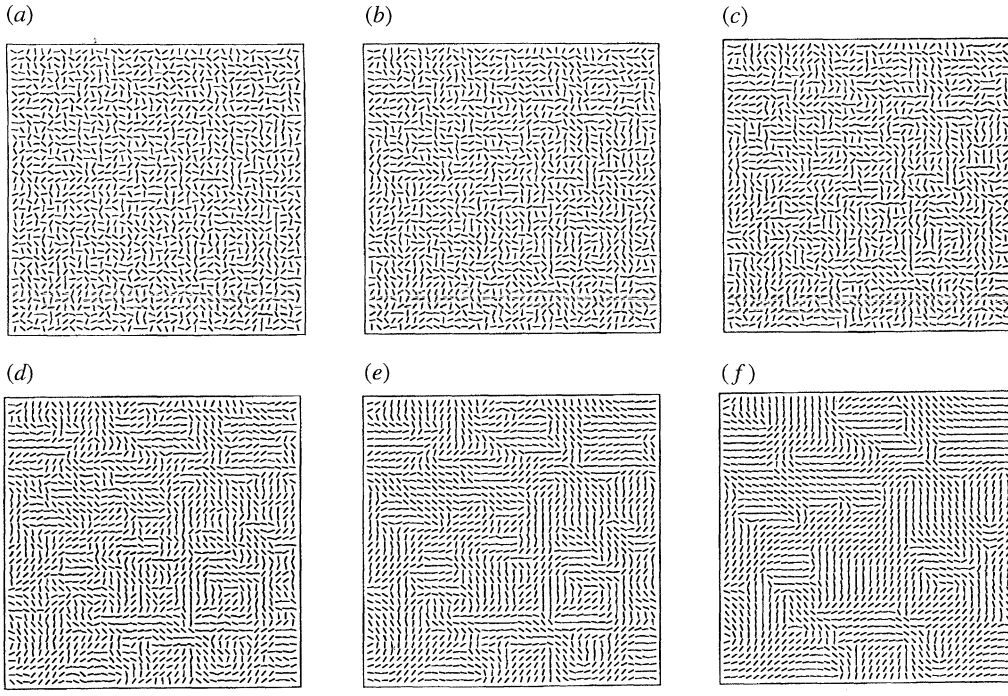

Figure 17. Director maps showing the effect of the director correlation process on an initially random arrangement of cell directions. (*a*) Initial state. After (*b*) 1, (*c*) 2, (*d*) 5, (*e*) 10 and (*f*) 50 iterations of the correlation equation (6.1).

Figure 18 shows the effect of a high level of shear alone. Starting from the original equilibrium state of the director array (figure 18*a*) the material is subjected to a vertical shear strain γ given by $\gamma = st$ where s is the shear rate ($s = 10\,\mathrm{s}^{-1}$) and t the time increment ($t = 0.05$ s). After each pseudo-affine deformation one orientation correlation step is performed. Figure 18*b–d* shows the director map evolution up to a shear strain of 150 (300 iterations). These indicate that full director orientation has been achieved. In this simulation the defects have been removed by the shear. Figures 18*e*, *f* correspond to the director trajectories after the cessation of flow. The correlation coefficient algorithm is applied after each step with no further applied strain. Clearly once fully oriented, the material remains oriented.

The loss of defects in the model during shear is a consequence of the coarse nature of the periodic array. With shear, the size of the defects reduces until they can no longer be represented on the grid, at which time they vanish from the model. We therefore now arbitrarily introduce defects into the model which exist both before, during and after shear. This effect is achieved by 'fixing' a certain number of cells in their original configuration. In the case shown in figure 19, 20% of the cells are randomly chosen as having fixed orientation. With the application of shear (figure 19*b–d*) the free directors respond to the shear deformation but the fixed defects influence the orientation of their near neighbours. Figure 19*c*, *d* shows that a limiting saturating orientation appears to have been reached. On the cessation of shear (figure 19*e*, *f*) the fixed defects play a vital role as they now act as nuclei for the global disorientation of the array. As time evolves the local

PHILOSOPHICAL TRANSACTIONS OF THE ROYAL SOCIETY A MATHEMATICAL, PHYSICAL & ENGINEERING SCIENCES

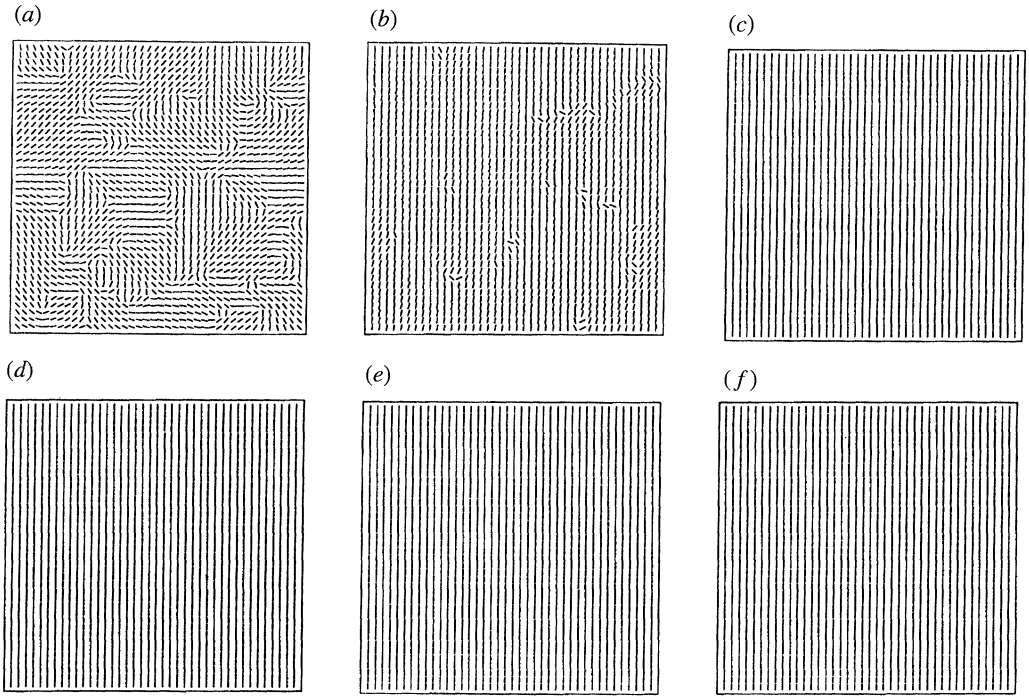

Figure 18. Director maps at various stages during the microstructural simulation of steady shear without defects. The shear rate was $10\,s^{-1}$. (*a*) Initial state. (*b*) $\gamma = 2.5$, (*c*) $\gamma = 25$, (*d*) $\gamma = 150$ during flow. (*e*) 1 s and (*f*) 30 s after cessation of flow.

anisotropy is maintained but global isotropy develops. This behaviour is similar to that experimentally observed.

Figure 20 shows a similar situation to the previous simulation but in this case 'fixed cells' are assigned randomly during the simulation at a rate proportional to the current stress (see later) with each lasting for a time proportional to the mean time constant for the material. We name these 'stress-induced defects' and again they correspond to our experimental observations. The simulations shown in figure 20 appear generally similar to those shown previously in figure 19 for the fixed defects. Combinations of fixed and stress-induced defects also showed little difference with each of the previous cases.

The overall degree of orientation that can occur for any of the director maps shown may be expressed as an orientation function S, using the average second Legendre polynomial:

$$S = \langle P_2(\theta) \rangle = \left\langle \tfrac{1}{2}(3\cos^2\theta - 1) \right\rangle, \tag{6.2}$$

where θ is the angle between the director in a cell and the shear direction.

Figure 21*a* shows the development of S with time for different shear rates when *no defects* are present, shear being stopped at $t = 30$ s. At a shear rate of $10\,s^{-1}$ the orientation function, which is reflecting the maps shown in figure 18, essentially follows a pseudo-affine deformation curve, reaching a final orientation of unity, reflecting the local orientation of the unit cells. The order parameter calculated here is the order parameter of the directors alone and full ordering gives $S = 1$. If there was some local disorder about the director of say $S_d = 0.8$ the final order

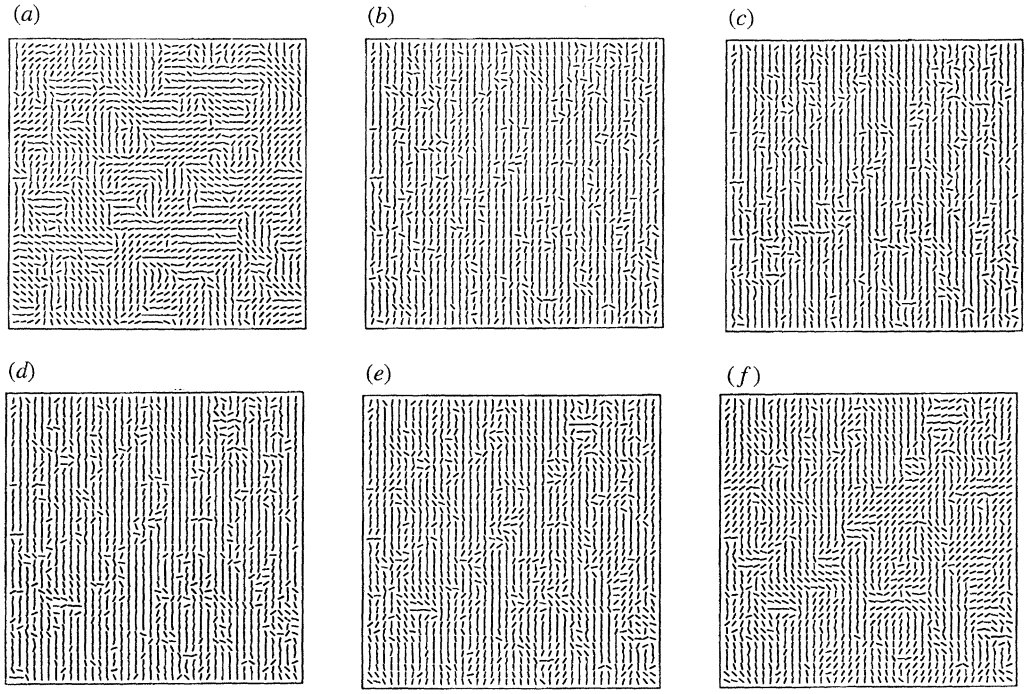

Figure 19. Director maps at various stages during the microstructural simulation of steady shear with fixed defects. The shear rate was $10\,s^{-1}$. (*a*) Initial state. (*b*) $\gamma = 2.5$, (*c*) $\gamma = 25$, (*d*) $\gamma = 150$ during flow. (*e*) 1 s and (*f*) 30 s after cessation of flow.

parameter of the assembly S_t would be $S_t = SS_d = 1 \times 0.8 = 0.8$. The $10\,s^{-1}$ shear rate curve also shows the important result that, when full orientation is achieved and the flow stopped at $t = 30$ s, the orientation does not change with further time elapse.

At low shear rates the directors have time to relax somewhat between each time step of deformation with the result that the S value reached is significantly less than unity. All simulations started from an initial condition where $S \sim 0.24$.

Figure 21*b* shows the time evolution of S for different shear rates when *fixed defects* are present. The $10\,s^{-1}$ curve is following the previously mapped behaviour of figure 19. In this situation flow induced orientation rapidly develops but the value of S saturates at a value of 0.8 because the presence of the defects is causing some disorientation of the directors. On the cessation of flow at $t = 30$ s global orientation relaxation can now occur because the directors have to adjust to the randomly oriented defect cells. The defects play an essential role in the global disorientation on the cessation of shear. At lower shear rates of 0.1 and $1\,s^{-1}$ the flow is too weak to cause significant orientation.

The model developed so far is now capable of describing to a first approximation the gross features of both the optical and the X-ray observations.

(*c*) *Rheology*

We now wish to incorporate the rheological response into the model and in order to do this anisotropic viscoelastic properties are assigned to each cell, following the aggregate model (Ward 1983; Green *et al.* 1990). The anisotropy of elasticity

PHILOSOPHICAL TRANSACTIONS OF THE ROYAL SOCIETY A MATHEMATICAL, PHYSICAL & ENGINEERING SCIENCES

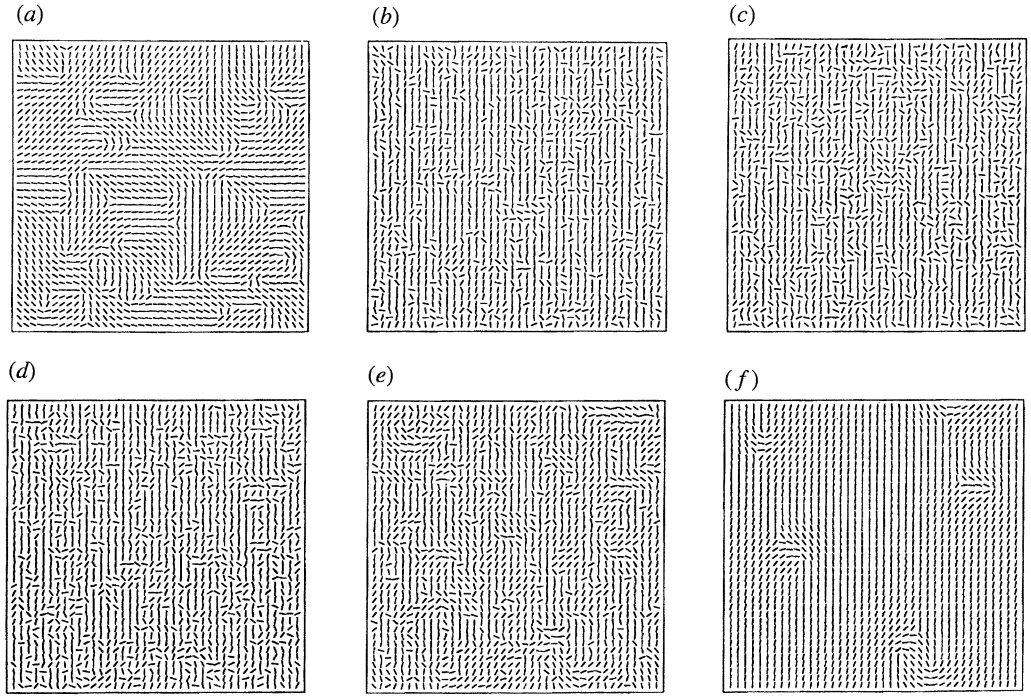

Figure 20. Director maps at various stages during the microstructural simulation of steady shear with shear-induced defects. The shear rate was $10\,s^{-1}$. (*a*) Initial state. (*b*) $\gamma = 2.5$, (*c*) $\gamma = 25$, (*d*) $\gamma = 150$ during flow. (*e*) 1 s and (*f*) 30 s after cessation of flow.

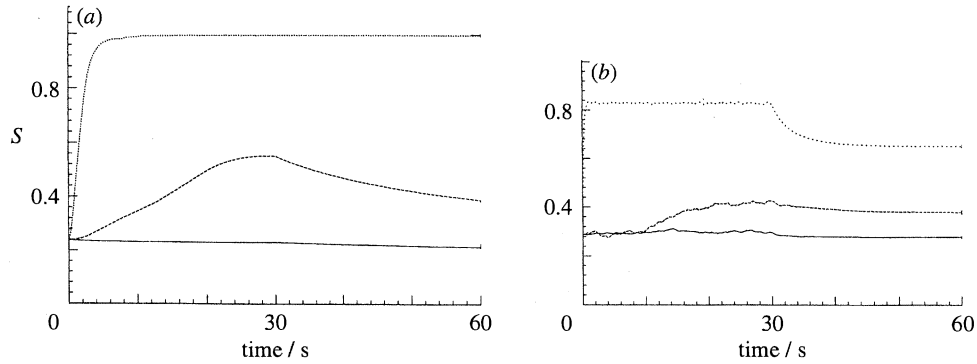

Figure 21. Orientation function calculated from the microstructural simulations. Shear ceases at time $t = 30$. (*a*) No defects included. (*b*) Fixed defects included. ———, $0.1\,s^{-1}$, - - - - -, $1\,s^{-1}$, · · · · · ·, $10\,s^{-1}$.

is a crucial assumption which we believe to be correct for liquid state TLCPs. There appears to be an underlying elasticity of TLCPs, in addition to the splay, twist and bend distortion energies present in SMLCs. Because a director can be defined within the melt and there is a preferred molecular orientation, it is reasonable to assume that the viscoelastic properties of the melt are anisotropic. Because our model at this stage is essentially phenomenological, it is not essential to assign the origin of elasticity to either entropic and/or internal energy contributions, although we suspect both mechanisms could be active.

PHILOSOPHICAL TRANSACTIONS OF THE ROYAL SOCIETY A MATHEMATICAL, PHYSICAL & ENGINEERING SCIENCES

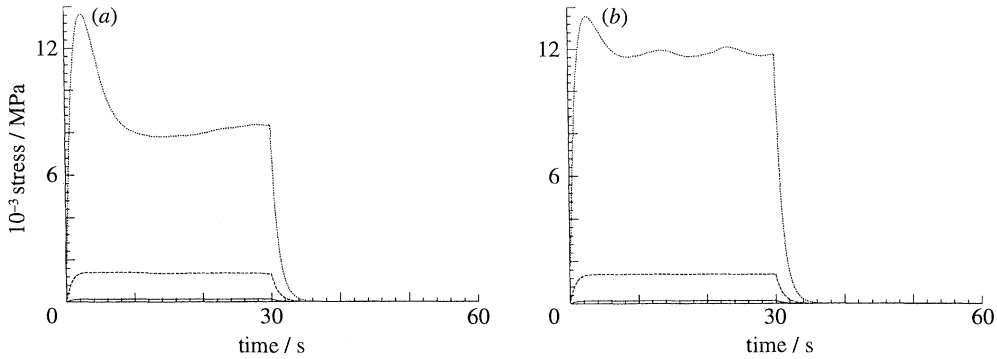

Figure 22. Steady shear data calculated from the microstructural simulations. Shear ceases at time $t = 30$. (*a*) No defects included. (*b*) Fixed defects included. ———, $0.1\,\mathrm{s}^{-1}$, - - - - -, $1\,\mathrm{s}^{-1}$, · · · · · ·, $10\,\mathrm{s}^{-1}$.

Assuming a uniaxial model, the elastic response of a single cell is described by two extensional moduli ($E_\parallel$ and $E_\perp$), a shear modulus (G_S) and two Poisson ratios (ν_1 and ν_2). We fix the ratio of the moduli somewhat arbitrarily at $E_\parallel : E_\perp : G_\mathrm{S} = 10 : 1 : 1$ and the Poisson ratios are fixed at 0.5. For any given cell director orientation, a tensor transformation is used to calculate the effective shear modulus of that particular cell at the specified orientation. Taking a random aggregate of units, a mean value of the shear modulus $\langle G \rangle$ is then calculated, yielding $E_\parallel$, $E_\perp$ and G_S in terms of $\langle G \rangle$.

We now identify $\langle G \rangle$ successively with each component value of shear modulus G_i that has been previously experimentally determined for a series of time constants using the G', G'' data (as shown in figure 12). In this way self-consistency with the experimental linear viscoelastic data is ensured and values of $E_\parallel$, $E_\perp$ and G_S can be determined for each time constant.

With a knowledge of the component values of the anisotropic modulus and given an arbitrary director map we can then determine the shear stress. For each time increment the average value of $\langle G \rangle$ is determined for the appropriate director map and the stress determined using the modified Maxwell equation,

$$\tau(t) = -\int_{-\infty}^{t} \sum_i \frac{\langle G_i(t') \rangle}{\lambda_i} \mathrm{e}^{-(t-t')/\lambda_i} \gamma(t, t')\, \mathrm{d}t', \tag{6.3}$$

where

$$\gamma(t, t') = \int_{t'}^{t} \dot{\gamma}(t'')\, \mathrm{d}t''.$$

$\langle G_i(t') \rangle$ is the shear modulus for each time constant component λ_i at the previous time t' averaged over all the cells and the integral is calculated as a sum over sufficient previous time steps for the required numerical accuracy. Thus as the director orientation map changes the $\langle G_i(t) \rangle$ components correspondingly change and modify the stress from simple Maxwell behaviour.

Examples of the predictions of the model are shown in figure 22. In figure 22*a* stress growth and relaxation curves are shown for different shear rates with no defects present. The director maps used in the calculations for $\dot{\gamma} = 10\,\mathrm{s}^{-1}$ were shown previously in figure 18. At low shear rates the stress increases to a constant

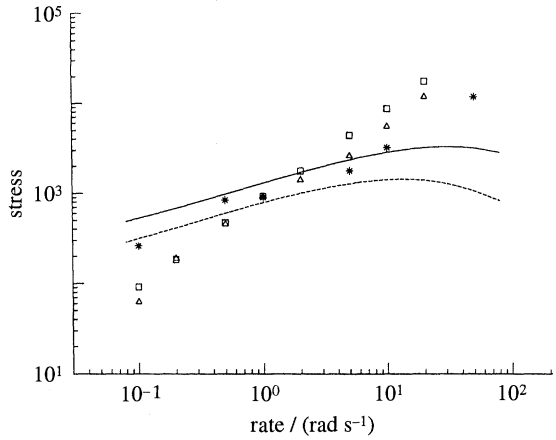

Figure 23. Comparison of experimental and modelled steady shear stress values. ∗, Experimental data from figure 15; △, microstructural model with no defects; □, microstructural model including defects. The lines are calculated from the constitutive equation (6.4) with two different values for k. ———, $k = 2$; - - - - -, $k = 4.6$.

value before stress relaxation at $t = 30$ s. At the higher value of $\dot{\gamma} = 10\,\mathrm{s}^{-1}$ a stress overshoot is predicted which is consistent with the experimental observations reported in figure 16. For all shear rates stress relaxation occurs with about the same timescale of a few seconds and it should be noted that the stress relaxation is very much faster than either the director disorientation after shear and the associated development of texture around defects if present.

Figure 22*b* shows an equivalent simulation to the previous figure but in this case fixed defects are present and the $\dot{\gamma} = 10\,\mathrm{s}^{-1}$ run corresponds to director trajectories shown in figure 19. The important observation here is that the presence of defects does not appear to significantly affect the kinetics of the stress build up or relaxation. At high shear rates the value of the steady shear stress is increased when compared to the no defect case and this is to be expected as the defects are acting as a local source of disorientation and hence enhanced $\langle G \rangle_i$. In all cases the simulation stress relaxation occurs over shorter times than texture relaxation.

Finally we compare results on the steady shear predictions with experimental data and the results are shown in figure 23. The experimental data are shown as stars and they are roughly in accord with a power law fluid, appearing as a straight line on a log–log plot. The square and triangle data correspond to the microstructural simulation described here for two cases where defects or no defects are present. Agreement for both situations is reasonable in the central shear rate region but poorer at both low and high shear rates.

We also show on the same graph the predictions of a Maxwell type constitutive equation which incorporates a Wagner type damping function (Wissbrun & Dealy 1990). This equation has the following form:

$$\tau(t) = -\int_{-\infty}^{t} \sum_i \frac{G_i}{\lambda_i} \mathrm{e}^{-(t-t')/\lambda_i} \mathrm{e}^{-k\gamma(t,t')} \gamma(t,t')\,\mathrm{d}t'. \tag{6.4}$$

Using the experimentally determined G_i from the G', G'' data and two different values of k taken from fitting different step strain data the predictions for steady

shear given by

$$\tau = \sum_i \frac{G_i \lambda_i \dot{\gamma}}{(1 + k\lambda\dot{\gamma})^2} \tag{6.5}$$

are also shown in figure 23. The fit with the experimental data is significantly worse than the microstructural simulation.

7. Discussion and conclusions

In this paper we have reviewed a range of TLCP response and have shown experimentally that the optical and texture behaviour of TLCPs resemble that of SMLCs rather than flexible polymers, however, the base rheology of the fluid is closer to that of flexible polymers. Clearly elements of local anisotropy and viscoelasticity play a role in describing the behaviour of TLCPs and their coupled effect has resulted in complex behaviour.

We have described results from two optical shearing devices both of which have been successful in obtaining information on oscillatory deformation and the rotational device for steady shear behaviour. The rotational device was used for both *in situ* optical and X-ray observations working in a temperature range of 200–320 °C. Our X-ray results show conclusively that TLCPs can be aligned by shear flow but perhaps surprisingly the overall level of orientation with $S \sim 0.8$ is quite low when compared to a magnetic field induced orientation of $S = 0.97$ at 5.6 T (Anwer & Windle 1993) and orientation levels in drawn solid LCP fibres. Our melt flow values are, however, similar to that found by Picken *et al.* (1990) for a Lyotropic LCP.

Our optical observations illustrate that defects within the material can play a major role in controlling overall orientation, particularly in the quiescent state and during relaxation after shear. Shear induces orientation as seen by both the X-ray data and optical birefringence. Shear also appears to lead to disclination multiplication. On the cessation of shear the presence of defects causes the oriented directors to reorient and the correlation coefficient model presented here appears to mimic this behaviour reasonably well. Our modelling of the defect texture is of course extremely crude; however, it does incorporate an important element in that it provides a mechanism for global orientation relaxation.

The rheology reported is representative of a number of TLCPs and its small strain linear viscoelastic response is close to that of flexible polymers. The material is viscoelastic with a broad range of relaxation times and can be modelled successfully by using a spectrum of time constants. The strain softening behaviour as revealed by the step strain experiment is generally more extreme than conventional flexible melts but the steady shear behaviour appears quite similar to conventional melt processing, showing a power law behaviour. Stress relaxation after steady shear was observed to be significantly faster than optical relaxation.

Both the microstructure and rheology of TLCPs have been shown to be complex and the realistic chances of developing a molecular model that fully describes deformation and flow of these materials at present seem remote. A phenomenological description of SMLCs has been successfully developed by Leslie (1983) but this at present cannot handle complex defect behaviour. Flexible polymers are adequately described by, for example, Doi & Edwards (1986), but again it is difficult to see how local orientation correlation and defect behaviour can be in-

PHILOSOPHICAL TRANSACTIONS OF THE ROYAL SOCIETY A MATHEMATICAL, PHYSICAL & ENGINEERING SCIENCES

corporated. Doi (1981) and Marruci & Maffettone (1989) have both developed molecular theories for LCPs but again these do not at this stage predict or include defect effects (see, for example, Larson 1988).

In this paper we have developed a director simulation that incorporates our experimentally observed optical observations. It is predictive but contains a number of semi-arbitrary adjustable parameters which as yet are not directly linked to molecular parameters The model has already been shown to predict observed quiescent defect textures (Bedford *et al.* 1991) and in this paper we have incorporated both shear and rheology. The constraints to obtain self consistency with optical, X-ray and rheological data are considerable and the model presented here does achieve this to a first approximation at least.

The main predictions of the simulation as presented here is that the presence of defects in particular influence orientation relaxation after shear and that the defects themselves do not appear to have a profound effect on rheology. The direct coupling of stress and orientation as reflected in the well-known stress optical coefficient for flexible polymers is therefore broken for TLCPs

We have constructed a mechanistic model that is guaranteed to be self consistent with the linear viscoelastic response in that we have accepted that the material contains a range of time constants and fitted the model to the linear viscoelastic data. The choice of the ratio of anisotropic tensile and shear modulus for each element is somewhat arbitrary although we found that changes of order four or five in these ratios did not have a major effect on the predicted results. Again the way in which defects were introduced into the model also did not significantly alter the rheological response. These observations collectively indicate that the rheology of the material is dominantly controlled by the intrinsic relaxation spectrum of the material together with the nonlinear response associated with the affine deformation of the director.

The simulation is pragmatic in that it reflects our experimental observations and does not directly correlate behaviour with either molecular mass or chain stiffness. The relaxation modulus that we have calculated from experimental G', G'' data will depend largely on the molecular mass distribution and, probably weakly, on chain stiffness, whereas the correlation coefficient ρ used in the simulation will depend dominantly on chain stiffness. We have had to arbitrarily introduce defects into the simulation but their presence will depend on both rheological and correlation parameters. The scope for further refinement and indeed solving equations from first principle is obviously considerable, however the magnitude of such an effort should not be underestimated.

Clearly the interplay between the anisotropic viscoelastic response introduced here and the Frank type elasticity that probably controls the disclination defect texture will require to be developed in the future. The mechanisms controlling the birth of disclination defect loops together with their multiplication during shear still needs to be clearly identified and incorporated into a fully consistent constitutive response.

We thank both SERC and Rhone Poulenc for financial support of this work and Alan Butcher for constructing both the translational and rotational shear cells.

References

Alderman, N. J. & Mackley, M. R. 1985 Optical textures observed during the shearing of thermotropic liquid crystalline polymers. *Faraday Discuss. Chem. Soc.* **79**, 149–160.

PHILOSOPHICAL TRANSACTIONS OF THE ROYAL SOCIETY A MATHEMATICAL, PHYSICAL & ENGINEERING SCIENCES

Anwer, A. & Windle, A. H. 1993 Magnetic orientation and microstructure of mainchain thermotropic copolyesters. *Polymer* **34**, 3347–3357.

Baumgaertel, M. & Winter, H. H. 1989 Determination of discrete relaxation and retardation time spectra from dynamic mechanical data. *Rheol. Acta.* **28**, 511–519.

Bedford, S. E., Nicholson, T. M. & Windle, A. H. 1991 A supra-molecular approach to the modelling of textures in liquid crystals. *Liquid Crystals* **10**, 63–71.

Blundell, D. J. 1982 The nature of crystallites in solidified, rigid-chain, liquid-crystal polymers. *Polymer* **23**, 359–364.

Doppert, H. L. & Picken, S. J. 1987 Rheological properties of aramid solutions: transient flow and rheo-optical measurements. *Mol. Cryst. Liq. Cryst.* **153**, 109–116.

Chandrasekhar, S. 1977 *Liquid crystals.* Cambridge University Press.

Chapoy, L. L., Marcher, B. & Rasmussen, K. K. 1988 The morphology of liquid crystal polymers and the possible consequences for their rheological behaviour. *Liquid Crystals* **3**, 1611–1636.

Cocchini, F., Nobile, M. R. & Aciemo, D. 1991 Transient and steady rheological behaviour of the thermotropic liquid crystalline copolyester 73/27 HBA/HNA. *J. Rheol.* **35**, 1171–1189.

de Gennes, P. G. 1974 *Physics of liquid crystals.* Oxford: Clarendon Press.

Doi, M. 1981 Molecular dynamics and rheological properties of concentrated solutions of rodlike polymers in isotropic and liquid-crystalline phases. *J. Polym. Sci. Polym. Phys.* **19**, 229–243.

Doi, M. 1992 Rheology of a system with mesoscopic domain structure. In *Theoretical and applied rheology: Proc. 11th Int. Cong. Rheology, Brussels* (ed. P. Moldenaers & R. Kennings), pp. 50–54. Elsevier.

Doi, M. & Edwards, S. F. 1986 *The theory of polymer dynamics.* Oxford: Clarendon Press.

Done, D. & Baird, D. G. 1987 The effect of thermal history on the rheology and texture of thermotropic liquid crystalline polymers. *Polym. Engng Sci.* **27**, 816–822.

Ferry, F. C. 1961 *Viscoelastic properties of polymers.* New York: Wiley.

Flory, P. J. 1969 *Statistical mechanics of chain molecules.* New York: Interscience.

Frank, F. C. 1958 On the theory of liquid crystals. *Discuss. Faraday Soc.* **25**, 19–28.

Graziano, D. & Mackley, M. R. 1984*a* Shear induced optical textures and their relaxation behaviour in thermotropic liquid crystalline polymers. *Mol. Cryst. Liq. Cryst.* **106**, 73–93.

Graziano, D. & Mackley, M. R. 1984*b* Disclinations observed during the shear of MBBA. *Mol. Cryst. Liq. Cryst.* **106**, 103–119.

Green, D. I., Unwin, A. P., Davies, G. R. & Ward, I. M. 1990 An aggregate model for random liquid crystalline copolyesters. *Polymer* **31**, 579–585.

Guskey, S. M. & Winter, H. H. 1991 Transient shear behaviour of a thermotropic liquid crystalline polymer in the nematic state. *J. Rheol.* **35**, 1191–1207.

Jackson, W. J. & Kuhfus, H. F. 1976 Liquid crystal polymers. I. Preparation and properties of p-hydroxybenzoic acid copolyesters. *J. Polym. Sci. Polym. Chem. Ed.* **14**, 2043–2058.

Kamath, V. M. & Mackley, M. R. 1989 The determination of polymer relaxation moduli and memory functions using integral transforms. *J. Non-Newtonian Fluid Mech.* **32**, 119–144.

Kamath, V. M. & Mackley, M. R. 1990 The rheometric characterisation of flexible chain and liquid crystal polymers. In *3rd European Rheology Conference* (ed. D. R. Oliver), pp. 261–264. British Society of Rheology.

Keates, P., Mitchell, G. R., Peuvrel-Disdier, E. & Navard, P. 1992 X-ray scattering from a flowing polymer solution. In *Theoretical and Applied Rheology: Proc. 11th Int. Cong. Rheology, Brussels* (ed. P. Moldenaers & R. Kennings), pp. 540–541. Elsevier.

Hilltrop, K. & Fischer, F. 1976 Radial Poiseuille flow of a homeotropic nematic LC layer. *Z. Naturf.* A **31**, 800–807.

Larson, R. G. 1988 *Constitutive equations for polymer melts and solutions*, pp. 299–340. Butterworth.

Larson, R. G. & Mead, D. W. 1989 Time and shear rate scaling laws for liquid crystal polymers. *J. Rheol.* **33**, 1251–1281.

PHILOSOPHICAL TRANSACTIONS OF THE ROYAL SOCIETY A MATHEMATICAL, PHYSICAL & ENGINEERING SCIENCES

Larson, R. G., Mead, D. W. & Gleeson, J. T. 1992 Texture of a liquid crystalline polymer during shear. In *Theoretical and Applied Rheology: Proc. 11th Int. Cong. Rheology, Brussels* (ed. P. Moldenaers & R. Kennings), pp. 65–69. Elsevier.

Lehman, O. 1890 Einige Fulle von Allotropie. *Z. Krist.* **18**, 464–467.

Leslie, F. M. 1983 Some topics in continuum theory of nematics. *Phil. Trans. R. Soc. Lond.* A **309**, 155–165.

Lin, Y. G. & Winter, H. H. 1988 Formation of a high melting crystal in a thermotropic aromatic copolyester. *Macromolecules* **21**, 2439–2443.

Mackley, M. R., Pinaud, F. & Siekmann, G. 1981 Observations of disclinations and optical microscopy in a mesomorphic copolyester. *Polymer* **22**, 437–446.

Marrucci, G. & Maffettone, P. L. 1989 Description of the liquid crystalline phase of rodlike polymers at high shear rates. *Macromolecules* **22**, 4076–4082.

Mitchell, G. R. & Windle, A. H. 1982 Conformational analysis of oriented non-crystalline polymers using wide angle X-ray scattering. *Colloid Polymer Sci.* **260**, 754–761.

Mitchell, G. R. & Windle, A. H. 1988 Orientation in liquid crystal polymers. In *Developments in crystalline polymers* (ed. D. C. Basset), pp. 115–175. Elsevier.

Nicholson, T. M. 1989 Computer simulation of liquid crystalline anisotropic structures. *Mol. Cryst. Liq. Cryst.* **177**, 163–175.

Nicholson, T. M., Mackley, M. R. & Windle, A. H. 1992 Shear induced crystallisation in a liquid crystalline random copolyester. *Polymer* **33**, 434–435.

Picken, S. J., Aerts, J., Visser, R. & Northolt, M. G. 1990 Structure and rheology of aramid solutions: X-ray scattering measurements. *Macromolecules* **23**, 3849–3854.

Sawyer, L. C. & Jaffe, M. 1986 The structure of thermotropic copolyesters. *J. Mater. Sci.* **21**, 1897–1913.

Tanaka, A., Fukuda, M., Nagai, H., Shinohara, M. and Onogi, S. 1984 Rheo-optical properties of polyethylene films in the nonlinear viscoelastic region. *J. Polym. Sci. Polym. Phys. Ed.* **27**, 2283–2293.

Troughton, M. J., Davies, G. R. & Ward, I. M. 1989 Dynamic mechanical properties of random copolyesters of 4-hydroxybenzoic acid and 2-hydroxy-6-napthoic acid. *Polymer* **30**, 58–62.

Viney, C., Donald, A. M. & Windle, A. H. 1983*a* Optical microscopy of banded structures in oriented thermotropic polymers. *J. Mater. Sci.* **18**, 1136–1142.

Viney, C., Mitchell, G. R. & Windle, A. H. 1983*b* Optical microstructure of oriented liquid crystal polymers. *Polymer Commun.* **24**, 145–146.

Viney, C., Mitchell, G. R. & Windle, A. H. 1985 Biaxial optical properties of thermotropic random copolyesters. *Mol. Cryst. Liq. Cryst.* **129**, 75–108.

Wagner, M. H. 1979 Network theory of polymer melts. *Rheol. Acta.* **18**, 33–50.

Ward, I. M. 1983 *Mechanical properties of solid polymers.* Wiley.

Windle, A. H. 1982 Measurement of molecular orientation and structure in non-crystalline polymers by wide angle X-ray diffraction. In *Developments in oriented polymers* (ed. I. M. Ward), pp. 1–46. Applied Science.

Wissbrun, K. F. & Dealy, J. M. 1990 *Melt rheology and its role in plastics processing.* Van Nostrand, Reinhold.

Received 10 December 1992; accepted 23 July 1993

PHILOSOPHICAL TRANSACTIONS OF THE ROYAL SOCIETY A MATHEMATICAL, PHYSICAL & ENGINEERING SCIENCES

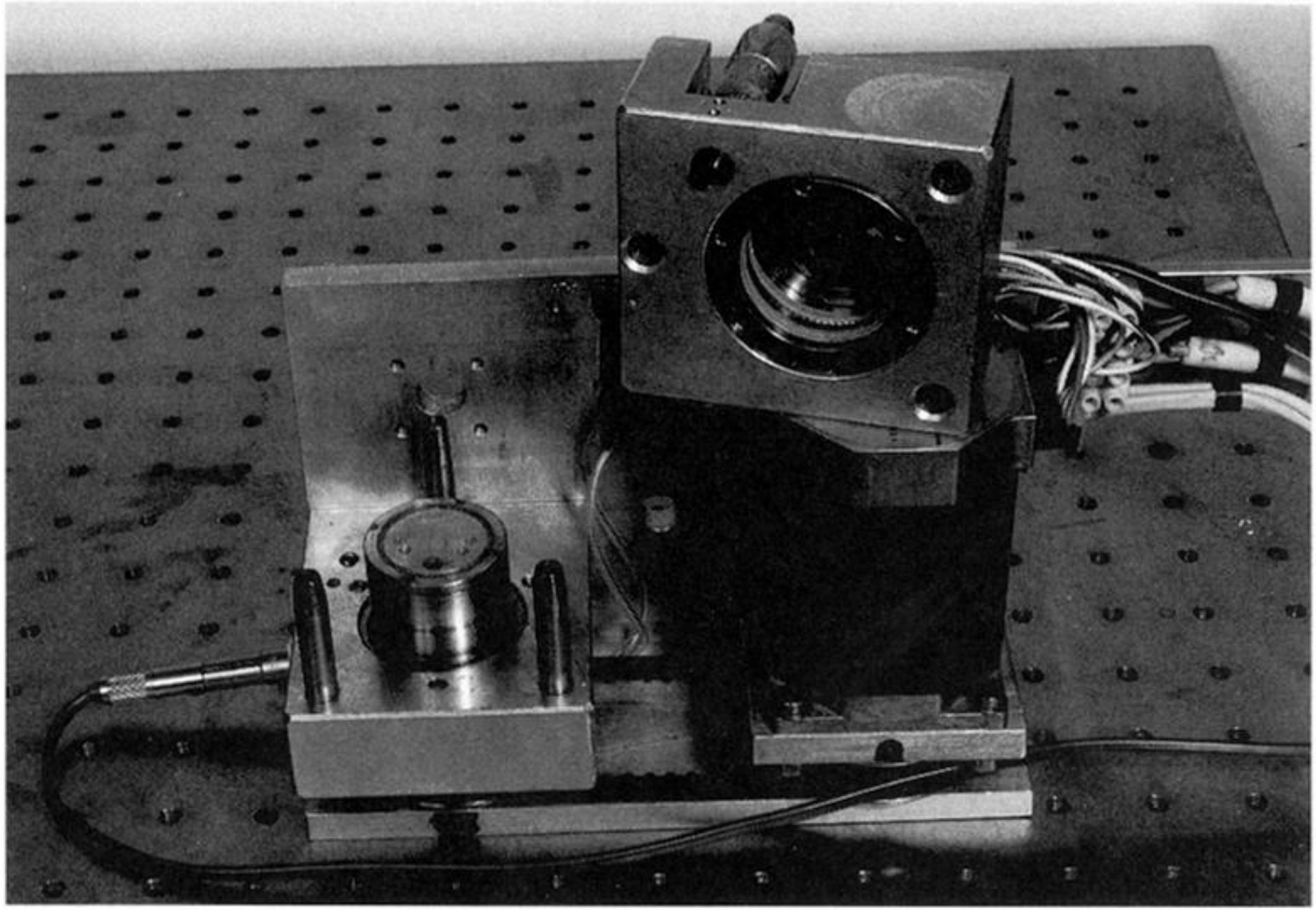

igure 3. Photograph of the rotational shear cell with the upper, stationary, window assembly removed.

PHILOSOPHICAL TRANSACTIONS OF THE ROYAL SOCIETY A MATHEMATICAL, PHYSICAL & ENGINEERING SCIENCES

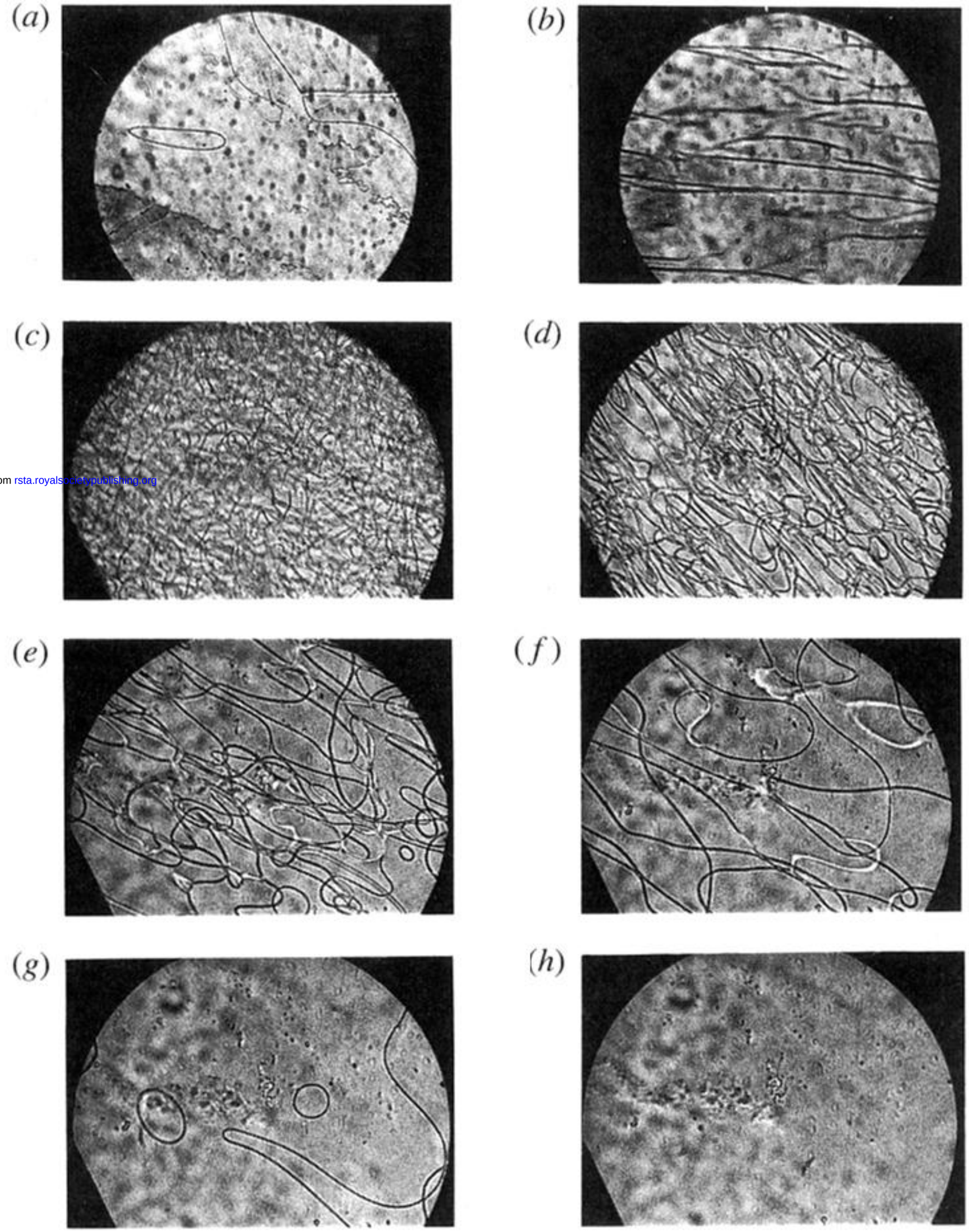

igure 4. Micrographs of MBBA. (*a*) At rest. (*b*) Shear rate $10\,s^{-1}$. (*c*) Shear rate $100\,s^{-1}$. *l*) 5s, (*e*) 10 s, (*f*) 30 s, (*g*) 1 min and (*h*) 2 min after cessation of shear. Direction of shear is orizontal.

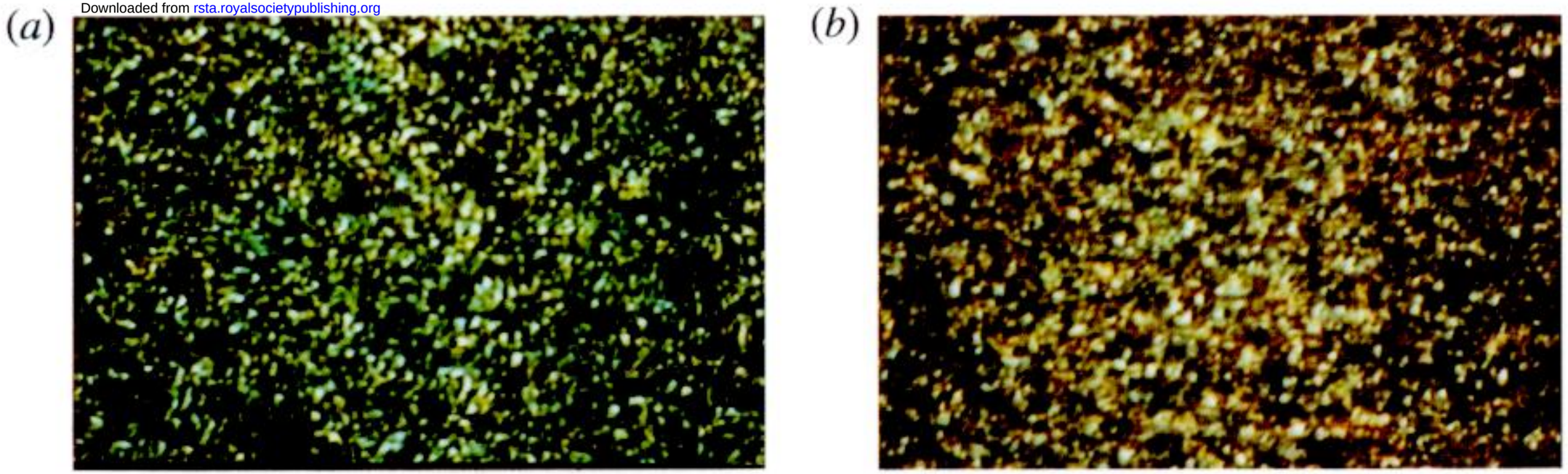

igure 5. Dense defect textures. All viewed between crossed polars. Thickness *ca.* 40 μm, width of ioto 250 μm. Annealing time 1 min. (*a*) Polymer B 220 °C, (*b*) Polymer C 315 °C, (*c*) Polymer A 0 °C.

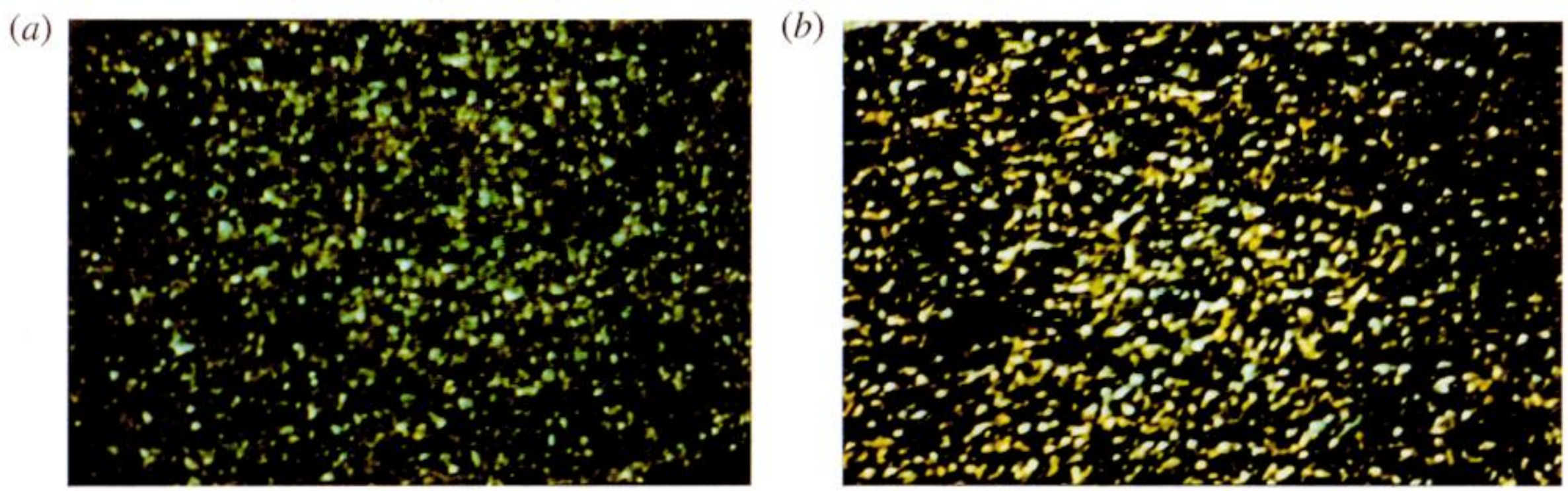

PHILOSOPHICAL TRANSACTIONS OF THE ROYAL SOCIETY A MATHEMATICAL, PHYSICAL & ENGINEERING SCIENCES

igure 6. Annealing of dense defect textures in Polymer B. All viewed between crossed polars. hickness *ca.* 40 μm, width of photo 250 μm. $T = 220$ °C. (*a*) 1 min, (*b*) 5 min, (*c*) 10 min, *l*) 12 min, (*e*) 15 min, (*f*) 20 min.

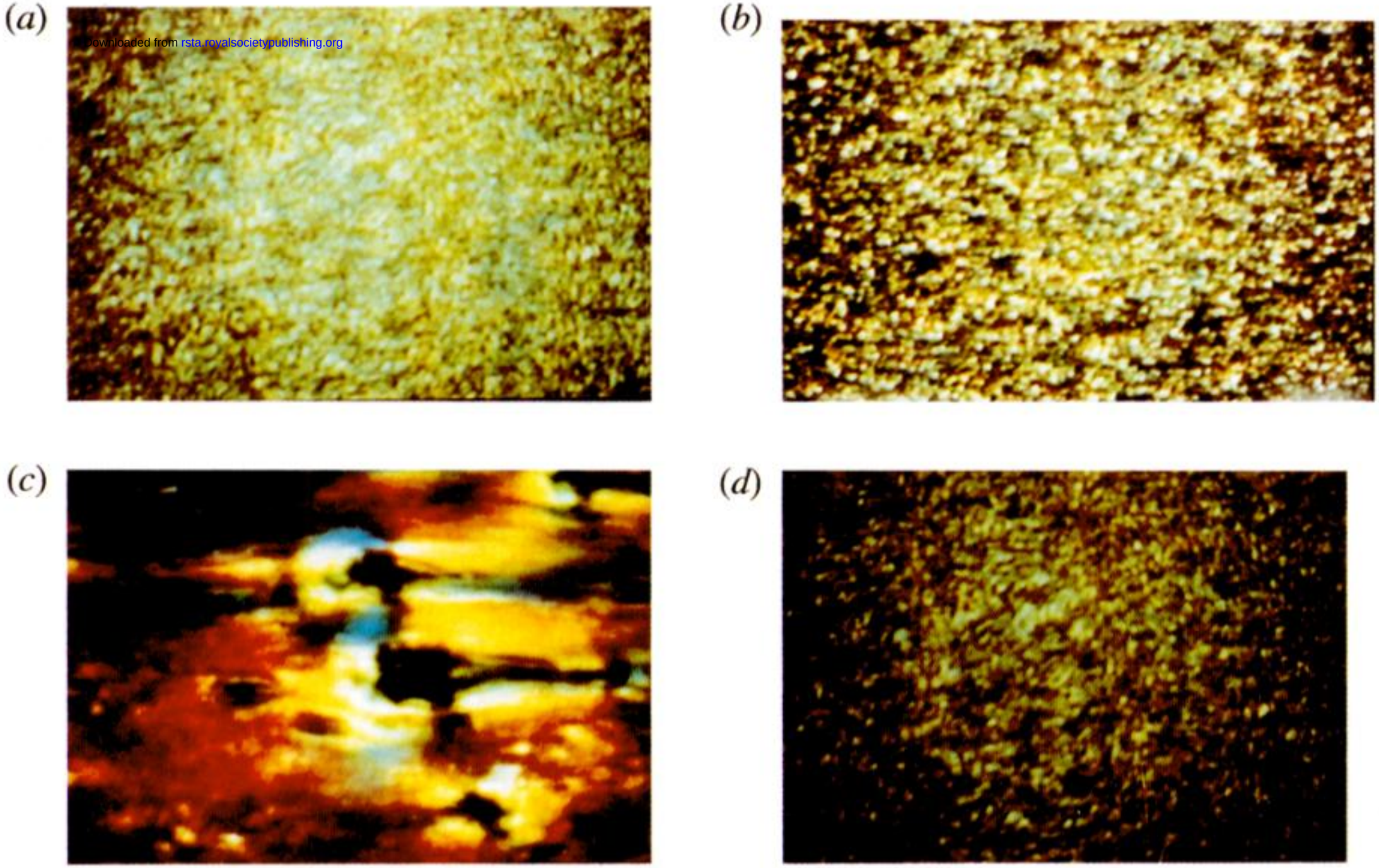

igure 7. The effect of shear on dense defect state in Polymer B 220 °C All viewed between ossed polars at 45° to horizontal oscillatory shear. Thickness *ca.* 40 μm, width of photo 250 μm, nealing time 1 min. (*a*) Quiescent state, (*b*) maximum shear rate 5 s^{-1}, (*c*) maximum shear te 150 s^{-1}, (*d*) 1 s after shear at 150 s^{-1}.

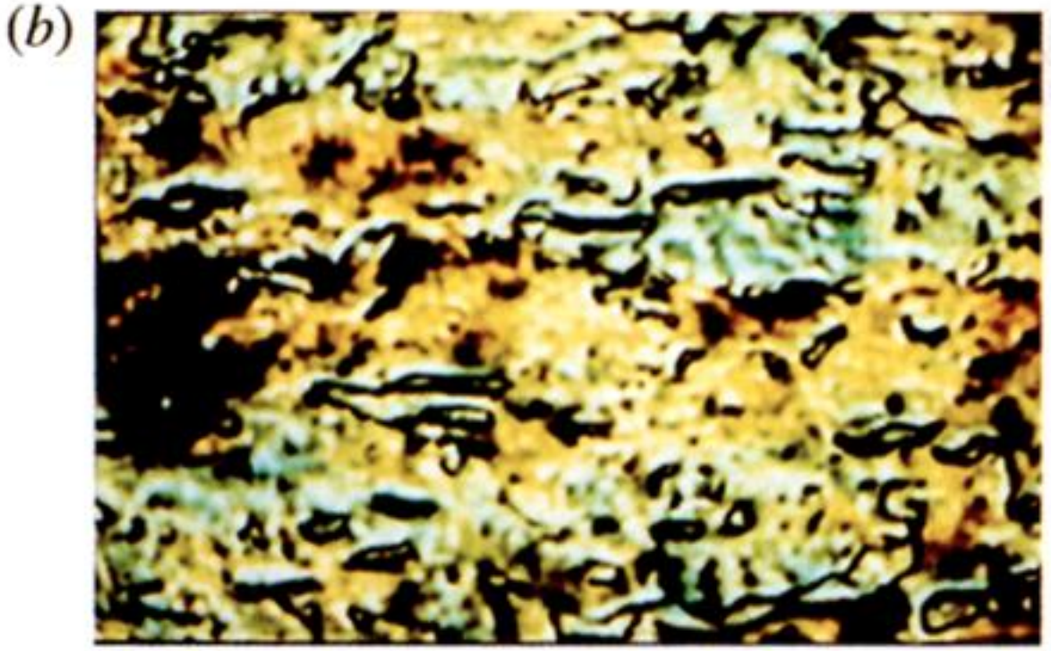

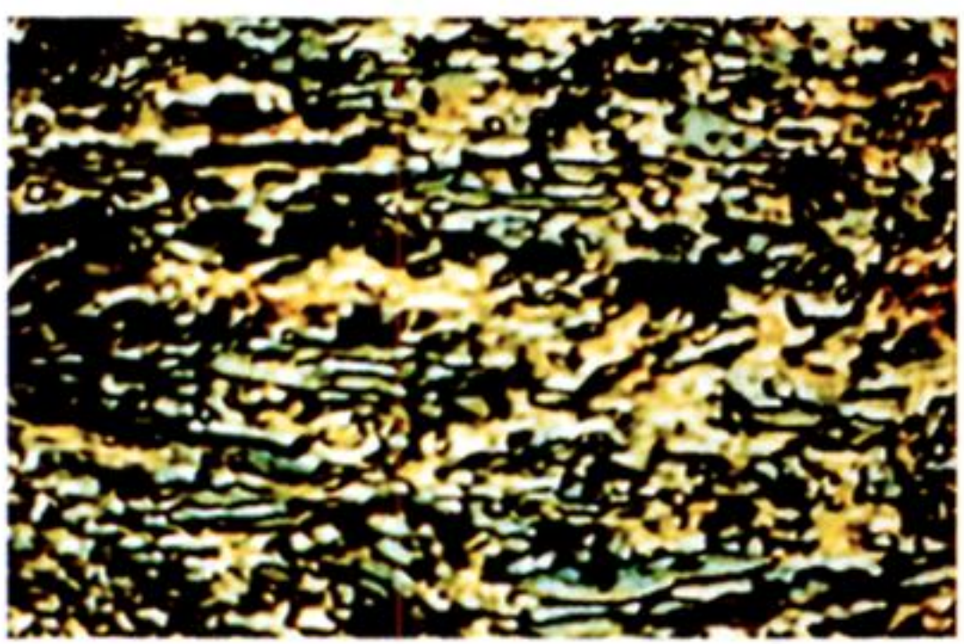

igure 8. The effect of shear on defect free state in Polymer B at 220 °C. All viewed between ossed polars at 45° to horizontal oscillatory shear. Thickness *ca.* 40 μm, width of photo 250 μm, nealing time 20 min. (*a*) Quiescent stage, (*b*) maximum shear rate 1 s^{-1}, (*c*) maximum shear te 10 s^{-1}, (*d*) maximum shear rate 150 s^{-1}.

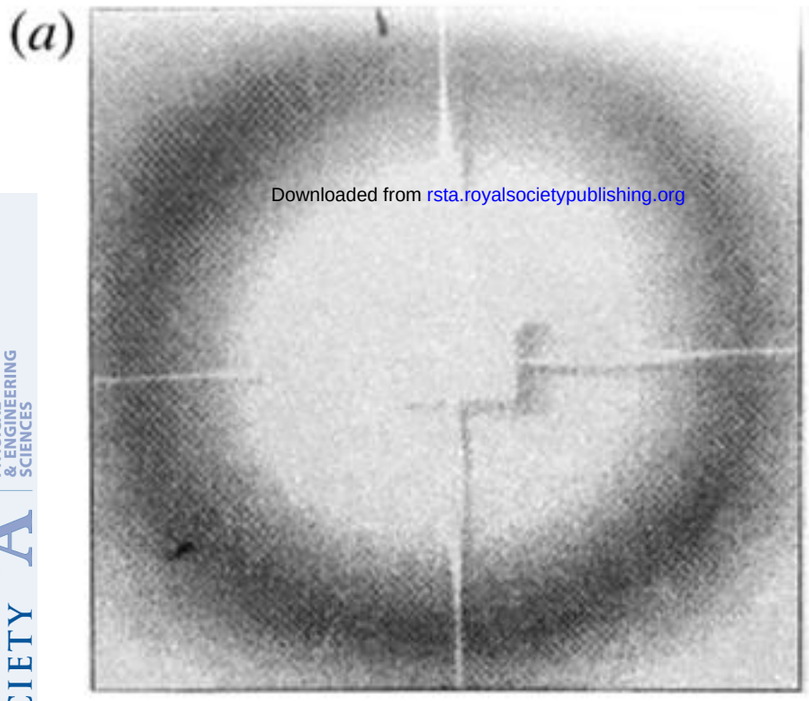

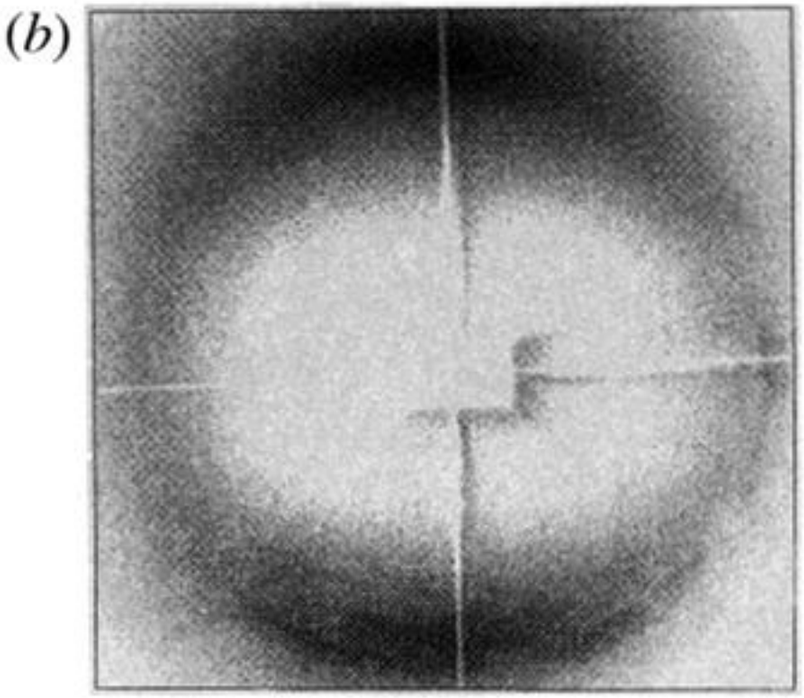

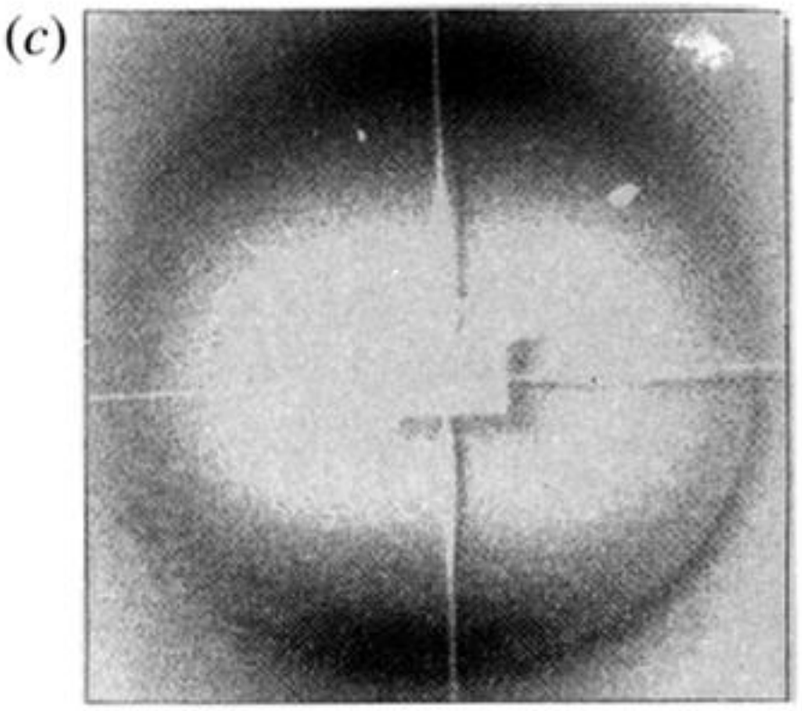

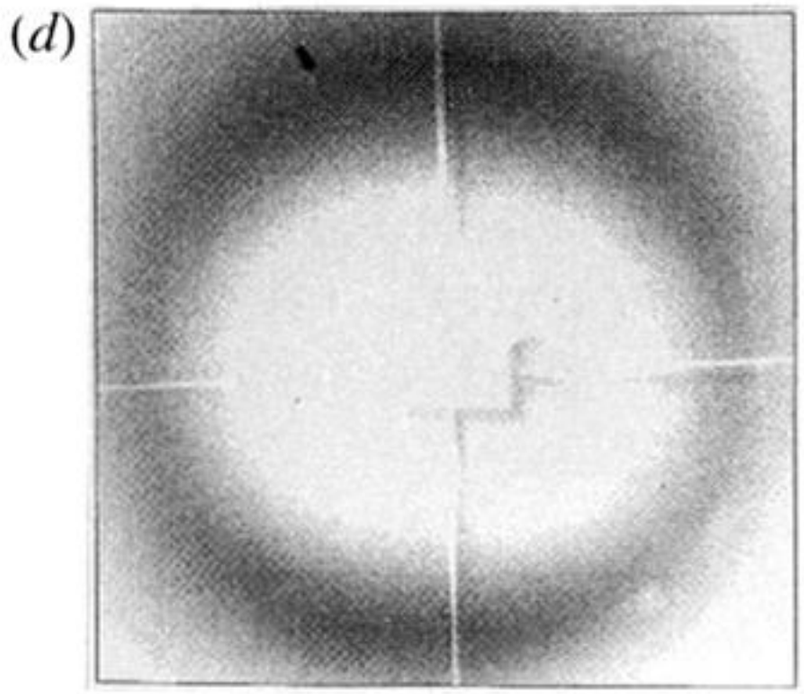

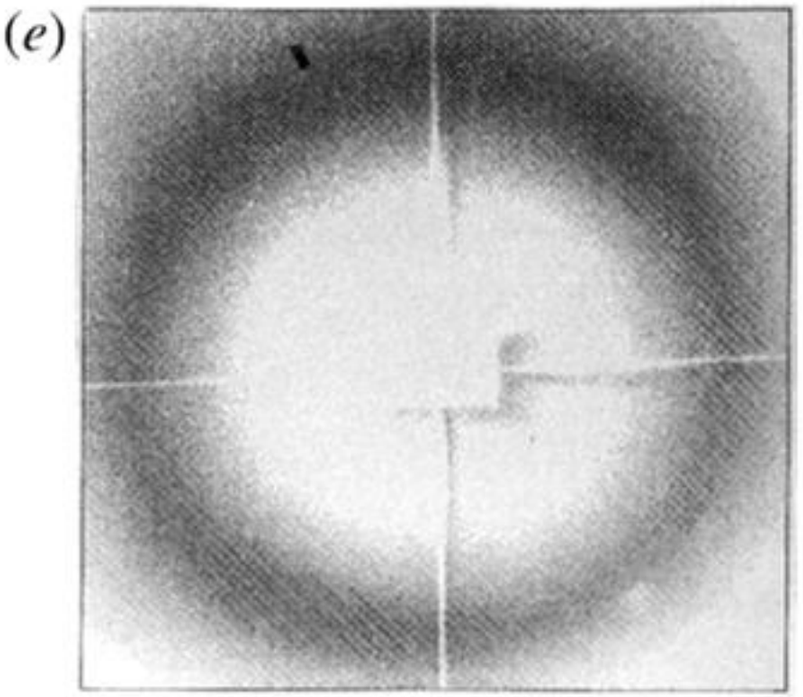

igure 9. Diffraction patterns of Polymer A collected at the Daresbury SRS. The shear direction horizontal. Temperature 310 °C. (*a*) At rest. (*b*) Shear rate $2\,s^{-1}$. (*c*) Shear rate $20\,s^{-1}$. *l*) 2 min and (*e*) 9 min after cessation of shear.